THESIS FOR THE DEGREE OF LICENTIATE OF ENGINEERING

Characteristics and Sintering of Fine Water-atomized and Carbonyl Iron Powder

JOHAN WENDEL

Characteristics and Sintering of Fine Water-atomized and
Carbonyl Iron Powder
Johan Wendel

Characteristics and Sintering of Fine Water-atomized and Carbonyl Iron Powder

Johan Wendel

Department of Industrial and Materials Science
Chalmers University of Technology

Abstract

Various types of iron powder are extensively use in the powder metallurgy (PM) industry. Water-atomized iron powder is commonly used as the base in many low-alloyed steel products manufactured through the conventional 'press and sinter' route, while carbonyl iron powder is often used for metal injection moulded (MIM) components. The two manufacturing methods share many similarities but differ in the powder shaping step where water-atomized iron powder is typically shaped by uniaxial die-compaction whereas the large fraction of organic material in MIM allows for a moulding step that enables higher component complexity.

The initial powder characteristics, such as the particle size, size distribution and morphology will largely determine the sintering behaviour of the powder grades. A fine, spherical powder has inherently higher sintering driving forces whereas coarse powder sinters to less extent. The chemical composition of the powder, especially the surface chemical state, will also play a role in sintering due to the enlarged surface area and reactivity of a powder. All iron powder particles are covered by a thin surface iron oxide layer that comprises the major fraction of the total surface area. The oxide layer contains a large amount of the total oxygen in the powder and furthermore acts as a barrier to diffusion that can hamper interparticle neck formation during the early stages of sintering. Consequently, the properties of the oxide layer are important for all subsequent processing of the powder. In addition to iron oxides, the powder contains oxidation-sensitive elements that are particularly vulnerable and tend to form oxide particulates that can deteriorate the mechanical properties of the components. Compaction of powder introduces deformation on a particle level, with heavily deformed regions localized to particle edges and where small sections of particles have a large fraction of their volume deformed. This is another factor that also influences sintering.

The scope of this study covers a number of methods to analyse the initial states of a given powder and compact in order to provide a foundation for its subsequent processing. Surface analytical techniques were used to determine some of the characteristics of the different powder grades in terms of the presence, composition and thickness of the surface iron oxide layer and oxide particulates. Additionally, the properties of the compacted green states were determined. Thermal analysis techniques were then used to provide information about how the powder interacts with the sintering atmosphere. The activation energy of the reduction of the surface iron oxide layer could be determined for both water-atomized and carbonyl powder, and nitrogen- and carbon-removal processes could also be shown for carbonyl iron. Furthermore, removal of internal oxygen in water-atomized powder by diffusion and subsequent reduction was identified. The sintering behaviour of compacted water-atomized iron powder and injection moulded carbonyl iron powder was then studied with dilatometry using a number of different processing parameters like initial compaction pressures, heating rates, and atmosphere composition. It was found that sintering is strongly affected by prior compaction, especially in the high-diffusivity ferrite region. High heating rates affect sintering of carbonyl iron powder to large extent, with a density increase at high heating rates. However, the heating rate also influences the chemical composition due to the altered interaction with the atmosphere.

Keywords: powder metallurgy, sintering, iron powder, surface analysis, thermal analysis, dilatometry

Preface

This work was carried out at the Department of Industrial and Materials Science, Chalmers University of Technology, Gothenburg, Sweden under the supervision of Professor Lars Nyborg and Professor Eduard Hryha. This licentiate thesis comprises an introduction to important aspects that need to be considered when discussing powder metallurgical treatments of water-atomized and carbonyl iron powder, with special emphasis on the surface quality of the powder, its thermal behaviour and the subsequent sintering.

List of appended papers

    I.   **Surface analysis of fine water-atomized iron powder and sintered material**
            J. Wendel, R. Shvab, E. Hryha, L. Nyborg
            Accepted for publication in Surface and Interface Analysis, ECASIA 2017 special issue

    II.   **Sintering behaviour of fine water-atomized iron powder – effect of initial green state**
            J. Wendel, S. Manchili, E. Hryha, L. Nyborg
            Manuscript, partly presented at Sintering 2017

    III.   **Sintering aspects of carbonyl iron powder**
            J. Wendel, R. Shvab, E. Hryha, L. Nyborg
            Manuscript, partly presented at Sintering 2017

Contribution to the appended papers

    I.   The author planned and performed parts of the experimental work and most of the analysis of the results. The author wrote the paper in cooperation with the co-authors.

    II.   The author planned and performed the majority of the experimental work, and analysed the results. The paper was written in collaboration with the co-authors. EBSD measurements were performed by Alexander Leicht.

    III.   The author planned and performed the majority of the experimental work and analysed the results. The paper was written in collaboration with the co-authors.

Papers not appended in this licentiate thesis

    a.   Sintering aspects of carbonyl iron powder used in metal injection moulding
            J. Wendel, R. Shvab, E. Hryha, L. Nyborg, D. Riabov, S. Berg
            Proceedings of World PM 2016
            An extended version of this conference paper was compiled into the manuscript of paper III.

Contents

Chapter I - Introduction

Powder metallurgy (PM) is commonly used as an umbrella term and refers to the scientific and technical aspects concerning metal powder, i.e. a collection of metal particles. The term refers both to the underlying physical and chemical principles that determine the properties of the powder material, and to the manufacturing processes in which the materials are fabricated and further processed into final products. The benefits of PM are that, compared to more traditional manufacturing methods such as casting and machining, the energy consumption and material waste can be kept to relatively low levels [1], while at the same time offering high throughput. The key lies in a process called sintering, in which the powder is brought to elevated temperatures at which the particles merge together by diffusion to densify the material and increase the mechanical properties. Today, the PM industry is significant and growing, although it is still small in relation to traditional metal-working. Indeed, PM is likely to remain a highly specialized industry used for dedicated applications. Ferrous powder metallurgy, i.e. iron-based material systems such as pure iron and various steels, comprise the major fraction of the world market of PM components. The automotive industry is a key customer, with PM presenting an competitive alternative manufacturing method for several applications [1].

The typical production process for many PM products is through the so called press-and-sinter route. The powder is first uniaxially compacted inside a die to attain the desired component shape. A lubricant is admixed to ease compaction by reducing friction between the powder and the die wall, and also between the powder particles [1]. The component, now in its "green" state, is removed and subsequently sintered. The sintering commonly takes place in large continuous belt furnaces with different heating zones. In the initial parts of the furnace, the lubricant is removed. This process is called delubrication and is a thermal degradation of the various organic species of the lubricant that takes place at an elevated temperature. Insufficient or failed removal of the lubricant can lead to contamination of the components. After delubrication, sintering of the compacts takes place at even higher temperatures at which material movement mechanisms through diffusion act to bridge the powder particles, thereby providing strength to the compacts. Careful control of the processing temperature profile and atmosphere is needed to ensure a satisfactory result of the delubrication and sintering.

The powder used in most PM processes are manufactured by atomization in which a stream of molten metal is disintegrated by jets of water or inert gases. The resulting particles are sieved and handled to create a relatively well-defined powder grade, with a nominal composition, morphology and particle size distribution. Because of the inherent properties of powder, it will exhibit certain behaviour that is unlike that of the corresponding bulk material. Over the years, a lot of effort has been focused on the powder properties and how they change during the sintering process, with reference to temperature and atmosphere interactions, see e.g. [2–6]. The overarching goal is to provide a robust manufacturing method with competitive advantages in some areas relative to the more traditional manufacturing methods. The increased specific surface area of a PM compact will e.g. dramatically increase its interaction with the surrounding atmosphere, which in turn is likely to cause more oxidation and corrosion. This process is accelerated at high temperatures, i.e. during delubrication and sintering. The surface conditions of powder, e.g. oxide layers and any impurity elements present, can severely inhibit sintering as particle surfaces come together, both by interfering with neck formation and creating a diffusion barrier between adjacent particles.

Objectives and Aims

The objective of this licentiate thesis is to provide further understanding of some critical aspects involved in processing of fine water-atomized iron powder for press and sinter powder metallurgy, and for carbonyl iron powder in a metal injection moulding context. The outcome of any powder metallurgical processing route is a function of the initial conditions as well as the processing parameters for each step in the production. Consequently, the complexity increases rapidly even for seemingly simple material systems.

Near-pure iron in different forms was chosen as a model system for the foundation of the study. The major parts are dedicated to the surface chemical analysis of powder of different grades with reference to their thermal properties and sintering behaviour. The focus of the work has been to understand the link between some of the fundamental aspects governing sintering, such as the initial conditions of the powder and compact, and the sintering conditions. Research questions formulated are:

- What is the initial surface state of the powder, and how does it respond to the sintering conditions, i.e. the temperature profile and atmosphere?
- What is the initial state of the green compact and how is it related to the sintering?

Particular interest is in the characteristics of the surface iron oxide layer that covers all metal particles. Despite the additional presence of particulate oxides, the surface layer constitutes the major fraction of the total powder surface area. In extension, iron oxide layers initially comprise the major fraction of interparticle contacts in a compacted powder. During the subsequent sintering, reduction of the iron oxide layer therefore governs when densifying mechanisms are initiated as exposed metal surfaces come into contact with each other, which is a requirement for sintering to proceed. Furthermore, a large fraction of the total oxygen is contained in the oxide layer which can influence particulate oxide growth at later stages in the sintering.

Densification by sintering is also determined by compaction effects as the metal particles are forced against each other, flattening contact points and increasing the area of the interparticle region. Furthermore, plastic deformation is thought to be involved in the initial stages of sintering.

The importance of the initial oxide reduction and the compaction-induced plastic deformation of metal powder particles are two important aspects during mainly the initial stages of sintering that necessitates further investigation.

Chapter II – Powder Metallurgy

Why powder metallurgy?

Two main selling points for powder metallurgy are the reduction of material waste and energy consumption compared to many other types of manufacturing processes, see Figure 1. The low material waste stems from the powder consolidation which, whether through injection moulding like in MIM, or through uniaxial pressing as in PM, can be considered net-shape or near net-shape. This means that the majority of the input material is part of the useful product and not discarded. A simple comparison is machining, where a lot of the starting material will be removed and has to be recycled. It should be noted that machining is an excellent, and often necessary, complement to PM when post-sintering finishing operations are required. The key to the energy savings commonly associated with PM lies in the net-shaping capability and the sintering process. Sintering allows for material bonding without the need of full melting as in the case of
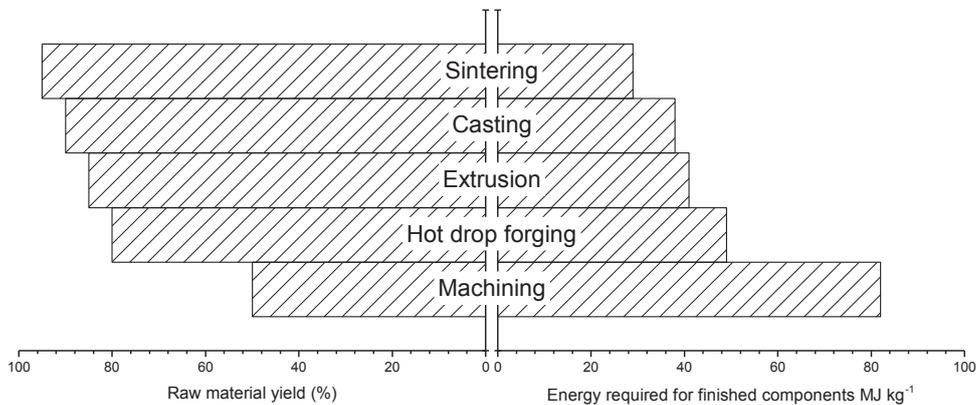

Figure 1: Raw material yield and energy consumption compared for some manufacturing methods. Redrawn from [1].
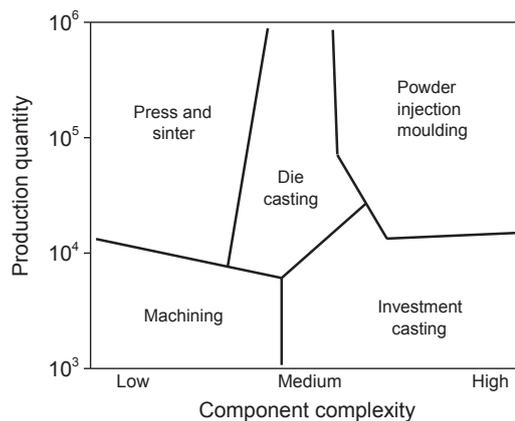

Figure 2: Schematic plot of the annual production quantity versus component complexity for some manufacturing methods. Redrawn from [14].

3

casting, and the process is also less energy-intensive than machining. Meanwhile, relatively good tolerance levels can be achieved [1].

Apart from the energy consumption and material waste, it is also important to look at the volume of production and the complexity of the components when choosing the manufacturing method. This is illustrated in Figure 2, in which favourable manufacturing methods are shown in relation to component production volume and complexity. Powder metallurgy techniques are typically used for high volume production of components with low to medium complexity for conventional PM, and medium to high complexity for MIM. The advent of additive manufacturing, also to some extent part of the PM family, allows for small series of complex components and is ideal for prototyping. The use of PM is either practically impossible or heavily disfavoured when the complexity of components is very low, such as for manufacturing of bars and sheets. Additionally, the component size of PM parts generally lies in the range of 0.05-2000 g, with limiting factors being e.g. the cost of the powder and the size and cost of the compacting press [1]. It is not a surprise, then, that PM remains a technology with limited potential to compete with traditional manufacturing methods in all but some specialized cases of components.

The mechanical properties of PM components are closely related to the porosity, which consequently is one of the main determinants for where the component is used. While the tensile strength scales linearly with porosity, properties related to dynamic behaviour, for example toughness and fatigue, does not. For such conditions, a density of over 7.5 g/cm^3 in ferrous components or above 95 % of relative density, is required which necessitates complementary processes like a second sintering step or hot isostatic pressing [1]. The corrosion resistance of PM steels are also typically worse than for wrought alloys owing to their porosity which enables crevice corrosion [7].

Special mention must be made regarding the material flexibility in PM. While ferrous alloys including iron and various steels comprise the majority of all PM products, some material systems rely heavily on PM concepts. Indeed, WC-Co cutting tool alloys are for example made through PM routes as a consequence of the high melting temperature of the constitutive elements where the Co-binder is liquid phase sintered to create the resulting microstructure [1].

In summary, PM offers competitive advantages in terms of energy savings and low material waste. The PM processes are ideal for high volume production of components ranging from low to high complexity and they offer a large material flexibility. Two drawbacks which limit the size of the components are the cost of the powder raw material and the tooling. As a result, PM does not necessarily replace traditional manufacturing methods, but complements them.

Classical 'press and sinter' powder metallurgy and metal injection moulding

This section will outline the basic processing steps of press and sinter and MIM, respectively, as they share many details. The steps can be summarized as powder mixing, shaping through compaction/moulding, delubrication/debinding and sintering.

Powder mixing

The choice of powder is the first question posed and of course determines the fundamental properties that the finished component will assume, i.e. iron powder makes an iron component. However, a detailed look on the powder characteristics indicates that the complexity can be high. This study is to large extent focused on the properties of various iron-based powder grades. The majority of iron-based powder grades are fabricated by means of atomization in which a stream of molten metal is disintegrated by jets of water or inert gases. When done with water, the powder is termed water-atomized, and it will be one main type of powder investigated here. The atomization determines many of the initial properties of the metal powder

such as its particle size, particle size distribution, morphology and surface chemistry. Water-atomized grades are commonly annealed to reduce the oxygen content, but even though most oxygen is removed, the powder will nonetheless contain oxygen due to the inevitable exposure to the surrounding atmosphere and possible residuals. Carbonyl iron is a completely different type of powder, made through the thermochemical carbonyl process, and the resulting powder has a much finer particle size, narrow size distribution, and spherical particle morphology. These properties make the powder suitable for MIM applications.

In the case of the press and sinter route, the powder is mixed with a lubricant to ease the subsequent powder shaping operation. The lubricant, which is typically an organic compound, reduces the friction both between the powder and the die and also affects the interaction between the metal particles. This is important as it ensures a homogenous particle distribution and increases the level of powder packing. The amount of lubricant is typically in the range of 0.3-0.5 wt.-%. For MIM, the organic compound is instead called a binder and amounts to a larger fraction of the mix, around 12 wt.-%. The volume fraction of powder in the blend is commonly referred to as a solids loading in MIM and is typically accordingly around 60 vol.-%. When the mixing is complete, the powder blend is ready for shaping operations.

Compaction/moulding
Shaping metal powder with techniques involving a compaction step, including e.g. uniaxial die compaction and cold isostatic pressing (CIP), relies on particle rearrangement and deformation of the powder particles to acquire a desired shape. The compaction initially leads to rearrangement of powder particles with an increase in pressure causing deformation to start at interparticle contact points. Further raising the pressure increases the number and size of the contact points which eventually leads to a high-density configuration of the powder [8]. The effect is more pronounced for ductile materials such as iron. At high compaction pressures, there is a transition from particle rearrangement to particle deformation which then becomes the main source of density increase [8–10]. Parallel to rearrangement and deformation of the metal particles, the number and size of pores is reduced which aids in the subsequent sintering process in which pores are eliminated to densify the material [8]. The deformation is partly elastic and partly plastic. Whereas the elastic deformation is relieved after the green compact is ejected from the die in a spring-back effect, the plastic deformation remains in the compacts [1].

Uniaxial die compaction inherently results in density gradients in pressed compacts. The density gradients are most prevalent along the surface regions of the compacts in the pressing direction. For uniaxial pressing there is a high relative density around the middle region, while this becomes a region of low relative density for compaction in two directions [1]. The density gradients in green compacts are a major cause of sintering anisotropy which can cause severe limitations in keeping component tolerances [11,12]. Fractured oxide layers at interparticle contact regions may also lead to oxygen trapping as the layers become enclosed within interparticle regions [13]. It is also likely that exposed surfaces below a cracked oxide layer can lead to some extent of re-oxidation.

Compaction methods such as CIP circumvents the issue of density gradients by providing a homogeneous density distribution in the compacts, which leads to more isotropic sintering behaviour. Higher green densities can also be achieved, since no lubricants are used. However, CIP has other issues related to it like poor tolerances and high tooling and die costs [1].

The MIM technology mitigates to some extent the inherent problems of compaction technologies, since the forming process does not involve any deformation of the particles. The large amount of polymeric binder allows the binder/powder mixture to be injection moulded in a similar way as polymers. Despite this, density gradients can occur if the moulding was done improperly, e.g. by not accounting for the density differences between the powder and the binder with respect to component design and flow characteristics [14].

Delubrication/debinding

The purpose of delubrication/debinding is, quite obviously, the removal of lubricants or binders used in either of the forming process. These additives are typically based on organic compounds which are removed by thermal decomposition. For MIM binders, more complex binder systems are also sometimes used, involving catalytic and/or solvent debinding. The debinding of MIM parts may thus include a multi-step procedure, combining an initial chemical dissolution step prior to thermal degradation [14].

Removal of lubricants can be a complex process, and failure is likely to be associated with problems that are often only revealed during the subsequent sintering, at which point there is low likelihood of addressing the issue. The decomposition process may lead to formation of products such as CO, CO_2 and H_2O, which risk to deteriorate the processing atmosphere [15]. While delubrication is fairly straight-forward on a lab-scale, knowledge of industrial scale delubrication processes is necessary to ensure robust production. On-line monitoring of e.g. delubrication has been promising [16], and further modification of the atmosphere to create a simulated dirty environment could be useful in predicting the delubrication and sintering behaviour [15].

Sintering

Sintering is not a new concept but has been known to humanity for several thousands of years. Indeed, sintering of metals took place as early as 3000 BCE [17]. At the time, sintering was born out of necessity since humanity was unable to attain high enough temperatures to perform casting of e.g. iron. When casting could be achieved through higher temperatures, sintering was largely forgotten and unused until the 18th century [17]. Sintering was then introduced for refractory elements, such as tungsten and tantalum, used in the early electronics industry of the 20th century, since the melting temperature of these elements was unattainable. Today, sintering is widely employed for metals when a specialized role can be filled, for example when the net-shaping capabilities of PM are beneficial.

Sintering is done at elevated temperatures, typically starting from 0.5-0.8 relative to the melting temperature of the material. Apart from the temperature the compacts experiences, and for how long, another crucial component for sintering is in which atmosphere the sintering takes place. How the atmosphere interacts with the powder being sintered is determined by the thermodynamic stability of the elements and their compounds under a given set of conditions.

At elevated temperatures, diffusion mechanisms become more active, which allows for increased movement of atoms. The minimization of the total surface area of the compacts is a key driving force of sintering in which metal particles are bridged and bonded together with so called sinter necks [8]. This driving force, however, is the dominant factor only for small micrometre-sized particles, e.g. powder used for MIM. For coarser powder grades, such as those used in the conventional press and sinter route, the driving force for minimization of surface area is less prominent, which consequently leads to less sintering. Despite this, sintering can be enhanced by increasing the number of contact points between particles, and even further by increasing the size of those contacts by compaction. By ensuring a high initial green density in this way, sintering can be realized by means of diffusion to yield good interparticle bonding. Concomitantly, provided that the sintering activity is high enough, atoms will move into pore structures, which will eventually leave the compact. The overall result is an increase in density and improved mechanical properties. Even so, improved properties will be gained even if densification is at a minimum, owing to surface diffusion effects that result in neck growth [18].

Ferrous powder metallurgy

Iron is arguably the most important engineering material in the history of humankind. Its combination with carbon to make steel is a particular success story with various steel grades being omnipresent not only in our daily lives, but also in the most remote places of humanity's reach.

Products based on iron and steel comprise the major fraction of the total PM market, with typical applications within the automotive industry, for engineering equipment, and more generally for the metal-processing industry [1,19].

Most iron-based components utilize water- or gas-atomized iron powder with water-atomized powder being more popular for plain iron and low-alloyed steels. Gas-atomized powder is generally used for high-alloyed steels, typically not used extensively in conventional PM, and will not be discussed more here. Carbonyl iron powder is fabricated through the carbonyl process and results in a very fine powder with narrow size distribution [26]. The scope of component production differs between regular press and sinter and MIM, with MIM finding use in certain mass-production areas including microfabrication [14,27].

Modern development in ferrous powder metallurgy of low-alloyed PM steels includes the transition from copper and nickel as alloying elements to steels containing chromium, manganese and silicon [4]. The reason for this is the desire to transition away from elements that can pose problems during recycling, e.g. copper, and whose price is relatively volatile, e.g. nickel and molybdenum [4,20]. While these new alloying elements are easily accounted for in conventional wrought steels, the increased surface area of powder will inevitably lead to complications during the subsequent powder processing and consolidation. The background is the altered thermal stability of the compacts as the new alloying elements readily form thermodynamically stable oxides that are more difficult to reduce than the iron oxides. Problems that arise during sintering are commonly observed [2,3]. Further complications include the reduction and re-oxidation of elements by the reduction products, as explained by oxide transformation mechanisms. However this is mainly critical in admixed systems which possess an inherent heterogeneity [21]. Segregation of various elements to particle surfaces has also been shown to alter the corrosion resistance of some PM steels, where oxide fractures promoted crevice corrosion [7].

While low-alloyed steels are commonly used in products, their constitutive materials are typically plain iron powder grades that are diffusion-bonded with fine powder of the various alloying elements or pre-alloyed powder grades with low content of alloying elements, typically limited to 3-5 wt.-%. One reason for the use of admixed systems is the high compressibility of the ductile base iron powder. Pre-alloying would instead solution-strengthen the steel prematurely, offering worse compaction which in turn would lead to lower sintered densities. While pre-alloying is possible for chromium due to its low solution strengthening effect in ferrite, an option for manganese is either mixing or by master-alloying techniques [4].

A number of studies has been done on iron powder pre-alloyed with these elements that form stable oxides [5,22]. A special interest has e.g. been taken in studying the transformation of the oxides during the sintering process, i.e. growth, change and interference with sinter neck formation [5,23,24]. While the surface of water-atomized powder has been studied previously, see e.g. [23], emphasis is often placed on the oxide particulates even though they comprise the minor fraction of the total surface. The chemical composition of the surface iron oxide layer is often considered to be only Fe_2O_3 although this is seldom the case. More extensive surface analyses can be utilized to determine the proportions of iron of different oxidation states in e.g. the surface oxide layer or in complex oxides [25]. If taken into account in combination with a kinetic analysis of the iron oxide reduction, a more complete description of the surface characteristics of water-atomized iron powder can likely be obtained.

Some problems with sintering theory is that even for simple model systems, the complexity increases rapidly. Sintering is influenced by a number of factors such particle size distribution, lubrication/binding and subsequent compaction [8]. Some of these are inherent to the powder and the effect of processing parameters is typically not considered. Water-atomized grades are generally expected have rather poor sintering activity when compared to carbonyl powder, which is a consequence of their much larger size [18]. In conventional PM, the goal of sintering is not usually to acquire a large density increase but to improve mechanical properties and keep tolerances. High green densities through compaction is therefore often preferred [1]. The case is different in MIM, where large shrinkages are needed for a large density increase with a simultaneous gain in mechanical properties. This can be achieved by the isotropic sintering expected in MIM [14].

Chapter III – Theoretical Considerations

This chapter aims to provide the theoretical framework that is needed for subsequent interpretation of the results. With a base in the principles that govern oxide formation and reduction for the relevant elements, an overview of diffusion and sintering mechanisms is then given for the present material system.

Thermodynamics and kinetics of oxidation and reduction in power metallurgical systems
The spontaneous dissociation of an oxide can be expressed

$$\frac{2}{y} M_x O_y = \frac{2x}{y} M + O_2 \tag{1}$$
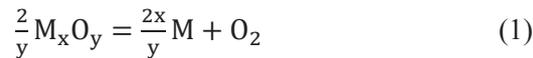
where M and O denote the metal and oxygen, respectively, and x and y balances the stoichiometry. The equilibrium constant for a reaction, K, is defined as the ratio between the activities of the reactants and products according to

$$K = \frac{a_M^{2x/y} \cdot a_{O_2}}{a_{M_x O_y}^{2/y}} \tag{2}$$

where a denotes the activity of the different species. For pure solids and compounds the activity is defined as unity whereas for gases the activity is equivalent to their partial pressures. Consequently, the equilibrium constant for the oxide dissociation becomes

$$K = p_{O_2} \tag{3}$$

The thermodynamic stability of an oxide under a given set of conditions can be expressed by its drive to break up into its reactants, i.e. metal and oxygen. For this reaction to take place spontaneously, at a constant temperature and pressure, the change in Gibbs free energy associated with the reaction, ΔG, must be negative. The change in G is related to a change in enthalpy and entropy at a given temperature T according to Gibbs equation

$$\Delta G = \Delta H - T\Delta S \tag{4}$$

A lower ΔG means a stronger tendency for the reaction to proceed. At equilibrium, $\Delta G = 0$, and the standard Gibbs free energy, ΔG^0, can then be derived to relate the thermodynamic stability of arbitrary compounds. The change in standard Gibbs free energy for a reaction is the difference in standard free energy between the products and the reactants following

$$\Delta G^0 = \sum G^0_{products} - \sum G^0_{reactants} \tag{5}$$

The standard Gibbs free energy change is related to the equilibrium constant of a reaction through

$$\Delta G^0 = -RT \ln(K) \tag{6}$$

where R is the gas constant. Combining Equations 3, 5 and 6 gives, with a = 1 for the metal and its oxide,

$$\Delta G^0 = -RT \ln(p_{O_2}) \tag{7}$$

Rewriting this leads to the expression

$$p_{O_2} = \exp\left(-\frac{\Delta G^0}{RT}\right) \tag{8}$$

Equation 8 describes the relation between the temperature and oxygen partial pressure conditions that are required to uphold equilibrium between the oxide and its reactants. The corresponding plots are shown in Figure 3 for a variety of different oxides that are important in powder metallurgical systems based on iron and low-alloyed steels. The plots were generated with the software HSC Chemistry 7.0.
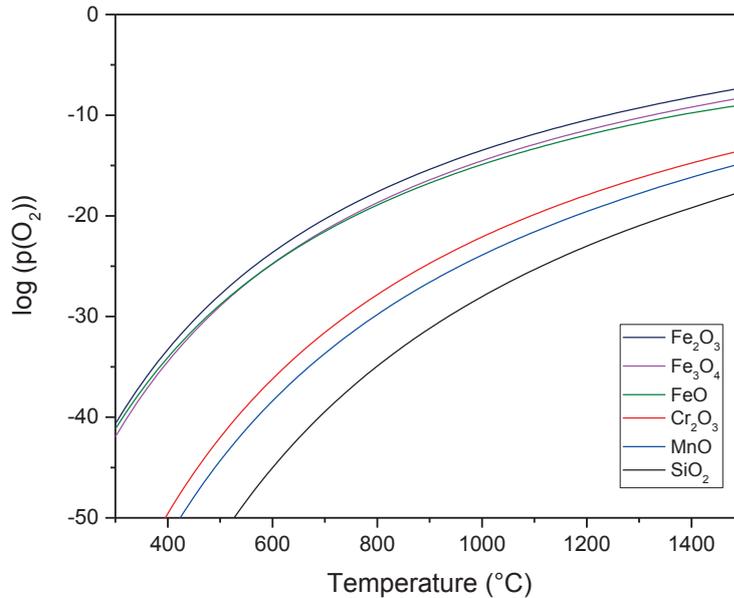

Figure 3: Oxide dissociation plot for some oxides commonly found in water-atomized iron powder grades used in powder metallurgy.

For conditions above each curve, dissociation of the oxide is favoured and it will spontaneously break up into its reactants. By either raising the temperature or lowering the oxygen partial pressure, it can be seen that oxide dissociation can be accomplished. It should be noted that thermodynamics alone does not explain when a specific oxide dissociation occurs, only if it is possible from a thermodynamic perspective. The kinetics of a reaction, which explains at what rate it takes place, must also be considered to fully understand how oxidation, dissociation and reduction occurs.

The positions of the curves in Figure 3 are related to the inherent thermodynamic properties of the elements and their oxides. It can be seen that the oxides of chromium, manganese and silicon have greatly varying thermodynamic stabilities. These elements are typically found either as alloying elements in certain low-alloyed PM steels, or as impurity elements in nominally pure iron powder. Relative to the three iron oxides, these oxides are all more stable, with silicon dioxide being the most stable oxide in this iron-based material system. Studies have pointed to the prevalence of various spinel oxides for low-alloyed steel [16], but they will not be discussed further here.

Oxide dissociation is easy in principle, but difficult in practice. Very high temperatures or very low oxygen partial pressures are required, making it unfeasible for most industrial applications where sensitive elements are involved. Nevertheless, vacuum sintering has found great use in e.g. the hard metal industry [28].

Instead, a reducing agent can be implemented, enabling reduction of the oxides at considerably more favourable conditions. The most common reducing agents in powder metallurgical processing are hydrogen and carbon, with carbon being able to reduce oxides via both direct and indirect carbothermal reduction mechanisms.

Utilizing hydrogen for oxide reduction results in the following expression

$$\frac{2}{y} M_x O_y + 2H_2 = \frac{2x}{y} M + 2H_2O \qquad (9)$$
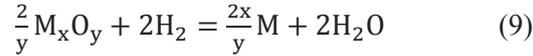
With reference to the discussion above and with Equation 2 altered for the presence of hydrogen, the following relation emerges

$$\frac{p_{H_2}}{p_{H_2O}} = \exp\left(\frac{\Delta G^0}{2RT}\right) \qquad (10)$$

The thermodynamic stability is now presented as the ratio of partial pressures of water vapour and hydrogen gas at a given temperature. Figure 4 presents the corresponding plots for the relevant oxides.
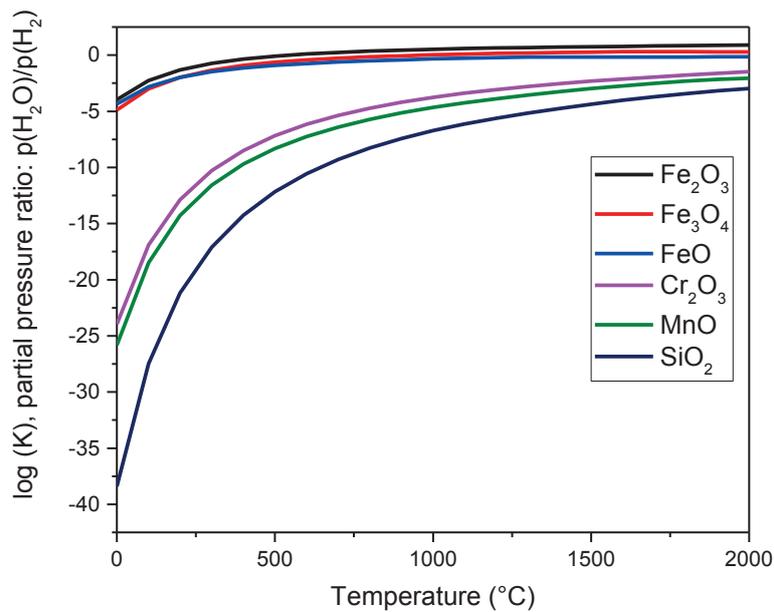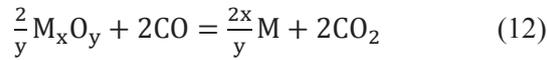

Figure 4: Reduction by hydrogen of some oxides commonly found in the present material system.

In this curve, the reduction proceeds for conditions below each curve, meaning that a certain ratio of hydrogen to water vapour is required. Again, it is seen that the various iron oxides are more easily reduced than the corresponding oxides of chromium, manganese and silicon. From the graph it can be seen that a hydrogen/water vapour ratio of only some 1000 is required to reduce iron oxide at 400 °C, whereas a ratio several order of magnitudes higher is required to reduce chromium and manganese oxides. For silicon oxide, the situation is even more critical. In summary, iron oxides are easily reduced in hydrogen at relatively low temperatures. For thermodynamically stable oxides, however, hydrogen is less effective and their reduction still requires a very large ratio of hydrogen/water vapour. Reduction by carbon is therefore a much more effective way to deal with stable oxides.

11

Reduction by carbon, termed carbothermal reduction, proceeds either via the direct or indirect mechanisms given by

$$\frac{2}{y} M_x O_y + 2C = \frac{2x}{y} M + 2CO \qquad (11)$$

$$\frac{2}{y} M_x O_y + 2CO = \frac{2x}{y} M + 2CO_2 \qquad (12)$$
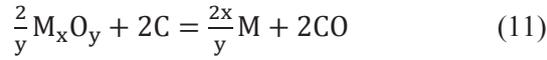
The corresponding relation becomes

$$\frac{p_{CO}}{p_{CO_2}} = \exp\left(\frac{\Delta G^0}{2RT}\right) \qquad (13)$$

Figure 5 shows the plots for the relevant oxides. Reduction takes place for conditions below each curve and compared to reduction by hydrogen it can be seen that the conditions, in terms of the required CO/CO_2 gas ratio, is less critical.
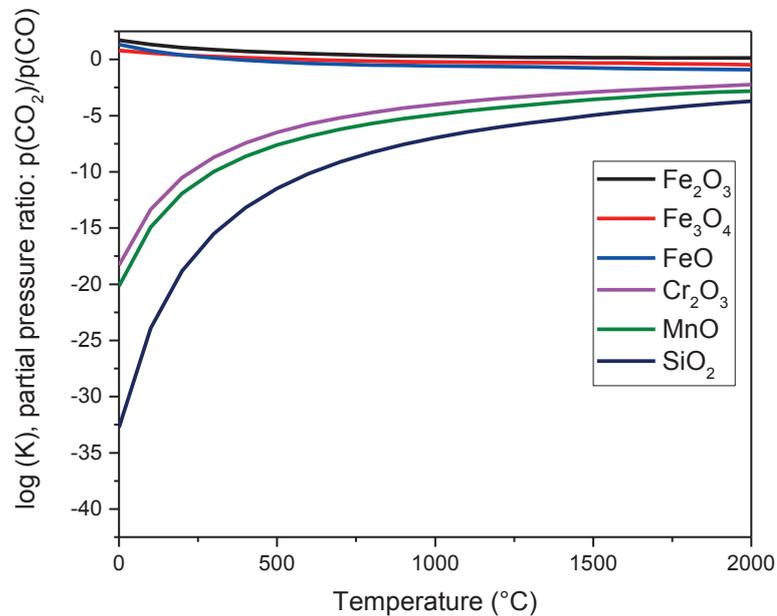

Figure 5: Reduction by carbon of some oxides commonly found in the present material system.

The thermodynamic stabilities of oxides are typically collected in a Richardson-Ellingham diagram, see e.g. [29], which provide an overview of the atmospheric conditions necessary to enable reduction of the oxide.

Both reduction by hydrogen and by carbothermal mechanisms are commonplace in many powder metallurgical contexts and their effect is well documented [3,30]. Cost is also an issue with hydrogen being expensive and also associated with handling risks. It should be noted here that the CO/CO_2 and H_2/H_2O ratios are always related for a given atmosphere via the water gas reaction ($CO + H_2O = CO_2 + H_2$) which means that they cannot be varied independently [5]. Great synergies between thermoanalytical techniques and mass spectrometry to identify and validate reduction processes have also been shown [31]. Studies of carbothermal reductions have e.g. been used to identify key temperatures at which reduction of the most common oxides take place. A complete reduction of iron oxides was identified to take place in the range 800-1050 °C, whereas the more stable oxides were reduced at higher temperatures. [32]. The removal of

oxygen is further complicated by oxide transformation mechanisms which refers to oxygen transfer between oxides of different thermodynamic stability. This is possible in localized regions of the compact pore structure where the local microclimate is simultaneously reducing and oxidizing to different oxides and instead of transportation away from the compact, the oxygen is simply transferred from one oxide to another [21]. The latter oxide then requires substantially higher temperatures for reduction, locking the oxygen in the compact [21]. The negative consequences was suggested to be partly impaired if sintering was conducted in hydrogen which facilitates a low-temperature removal of iron oxide, but this approach may be limited in an industrial setting due to interference with the delubrication process [21].

Kinetics of oxide reduction

The kinetics of a reaction involving mass loss can be analysed by performing a series of thermogravimetric experiments in which the heating rate is varied. This approach was first developed during the study of the drying process of various types of clay, giving information about the activation energies of the reactions [33,34]. The methodology has later been adopted more generally, including for studies of reduction of oxides [35,36], and thermal debinding processes [37]. The method is based on the temperature shifts that a reaction exhibits in response to a change in heating rate. A high heating rate shifts the reaction temperature to higher temperatures. The shift is defined by the difference in peak temperatures of the first derivatives of the mass loss curves, i.e. the mass loss rates. The following equation is typically used

$$\ln \frac{\Phi}{T_{max}^2} = \ln A - \frac{E_a}{RT_{max}} \qquad (14)$$

where Φ denotes the heating rate, T_{max} is the temperature at the peak of the first derivative, A is a pre-exponential factor, E_a is the activation energy and R is the gas constant. The activation energy describes the energy barrier for a reaction to take place and is a key parameter in general Arrhenius type relationships that define a number of processes

$$k = A\exp\left(-\frac{E_a}{RT}\right) \qquad (15)$$

where k is the rate constant of the reaction. Following the methodology developed here and applying it to the current powder metallurgy system can yield information about how e.g. the reduction of the surface iron oxide layer proceeds. Furthermore, it can be used to provide information about mass losses connected to diffusion and subsequent removal of oxygen within the powder. Since the oxide layer is not homogeneous and contains different oxides, multiple reactions take place. The reduction of haematite, i.e. Fe_2O_3, is typically reported as a step-wise reduction of the intermediate oxides of magnetite and wüstite, Fe_3O_4 and FeO, respectively, each step with separate activation energies [35]. Metal additives have also been shown to have a catalytic effect on the reduction [38], something that may be possible in the present case. However, the reduction described here is simplified to only include a single reduction step, with just one activation energy.

Diffusion

The importance of diffusion in metallurgical processes can hardly be overstated as this factor, together with thermodynamics and kinetics, governs how elements move across the material in search of equilibrium. As sintering is just movement of atoms, understanding diffusion is the key to understanding sintering.

Depending on the size of the diffusing element, the mechanism of material movement can be either that of substitutional diffusion or interstitial diffusion. Substitutional diffusion refers to the case when the solute atoms are similar in size to the atoms residing in the host lattice and can be located at one of the designated atomic positions. Interstitial diffusion refers to the case when the solute atoms are considerably smaller than the host atoms or for other reasons cannot move at these positions and instead move by jumping between

tetrahedral or octahedral voids in the crystal structure. For substitutional diffusion, the movement of atoms is relatively slow given the fact that there has to be positions that are unoccupied in order to allow the diffusion jump to be completed. This requires a vacancy in the lattice at the specified position. The vacancy concentration in turn depends on the material itself and the temperature. Interstitial atoms lack this hindrance as the solute concentration relative to the available lattice voids is low, making diffusion faster. When considering substitutional diffusivities in alloys, the movement of different elements will not be the same and each atomic species must be considered with a separate diffusion coefficient. This describes how the atoms will move relative to the host lattice [39].

The diffusion process is further complicated if the material exhibits allotropic transformations, i.e. a change in the crystal structure between two phases. Such is the case for iron, which undergoes a number of different transformations upon heating. For near carbon-free iron, the following phase transformations are passed

$$\alpha\,(\text{ferrite, bcc}) \xleftrightarrow{912\,°C} \gamma\,(\text{austenite, fcc}) \xleftrightarrow{1395\,°C} \delta\,(\text{ferrite, bcc})$$

The above phase transformations are valid for atmospheric pressure conditions. In addition to the three phases above, a fourth condition of iron exists at temperatures 770-912 °C and refers to the magnetic transformation from a ferromagnetic state to a paramagnetic state at the Curie point of ~770 °C. This is important because although there is no structural change in the crystal structure of the iron, the mechanisms by which self-diffusion is enabled is slightly altered, raising the diffusion rates to a level not explained purely by an extrapolation of the diffusion in the ferromagnetic state of ferrite, see Figure 6.
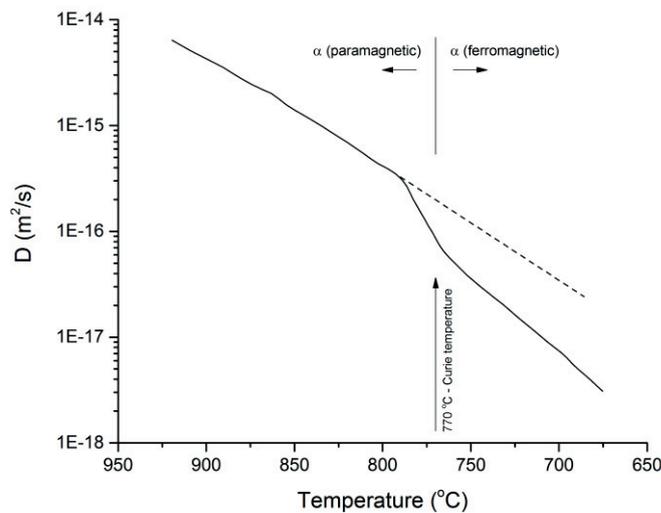

Figure 6: Volume self-diffusion in iron, highlighting the effect of the magnetic transformation on the diffusion behaviour. Redrawn from [40].

A large increase in the diffusion coefficient is reported to begin at the Curie point of 770 °C, changing the slope of the curve over a range before the diffusion coefficient then assumes a new slope during the remainder of the ferrite phase. The increase is related to the change in the magnetic domain structure of the iron when passing from a ferromagnetic to a paramagnetic state. Apart from a change in self-diffusion coefficients, the substitutional diffusion of other elements, e.g. chromium, is changed according to the effect on the host matrix [41]. The magnetic transition also affects other diffusion mechanisms in similar ways, albeit with different magnitudes. The diffusion coefficients of grain boundary and dislocation pipe diffusion

were noted to exhibit a significant decrease whereas the diffusion coefficient of volume diffusion was more moderate [41].

Furthermore, the diffusion coefficients also change at the allotropic phase transformation, i.e. the ferrite-austenite transformation. Only a small change in grain boundary diffusivities exists at the ferrite-austenite transformation temperature, whereas the gap in the magnitude for volume diffusion coefficients is considerably larger [40,42]. Additionally, segregation of impurity elements to grain boundaries significantly affects the grain boundary self-diffusion, one example being tin in high-purity iron [42].
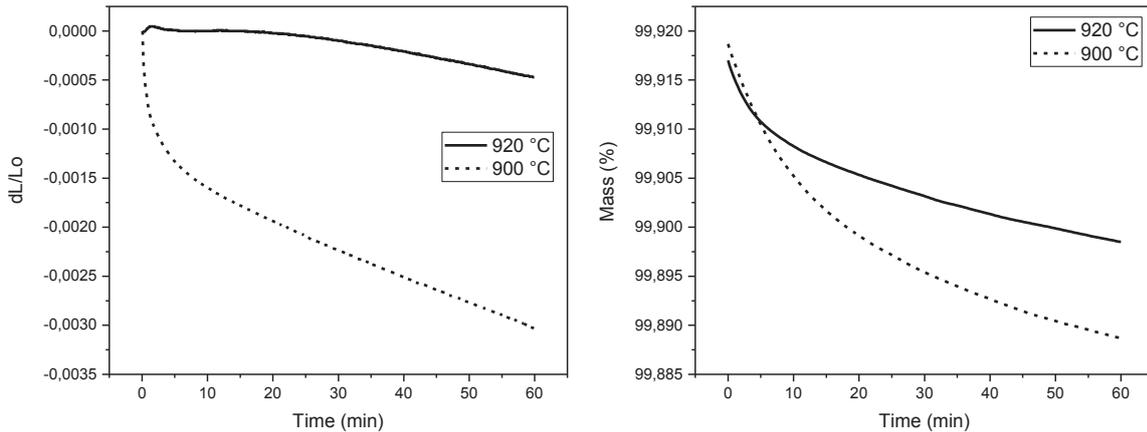

Figure 7: Left: Dilatometric and right: thermogravimetric curves illustrating the effect of crystal structure on the diffusion coefficients of iron self-diffusion and oxygen diffusion. Author's own results.

A sample curve is shown in Figure 7 (left), detailing two samples sintered at 900 and 920 °C, respectively. The results were acquired with a dilatometer. The sintering as a function of crystal structure is clearly illustrated. The bcc crystal structure of ferrite is more open than the fcc crystal structure of austenite and thus allows for a higher self-diffusion [39]. The phase dependence of grain boundary and volume diffusion also suggests that volume diffusion plays a significant role in the sintering of the present powder compact due to the large difference in dimensional change on either side of the transformation. Interstitial diffusion is also greatly affected by the crystal structure of the host lattice, with faster oxygen diffusion in bcc than in fcc, see Figure 7 (right).

In addition to diffusion along surfaces, grain boundaries and through the crystal lattice, diffusion can also take place through dislocation pipes in the iron matrix. While the contribution of pipe diffusion to the overall movement of atoms by other diffusion mechanisms is generally low, it can have a significant effect at low temperatures but also requires extensive deformation to generate the dislocations. Since the activation energy for pipe diffusion is less than for lattice diffusion, its contribution decreases less with a decreasing temperature, which allows the apparent diffusivity to become dominated by pipe diffusion along dislocations. At low temperatures the deformation state of the material may enhance the sintering through the dislocation pipe diffusion mechanism [43], but recovery and recrystallization will at some point render the effect negligible. Sintering experiments on aluminium powder showed that hydrogen caused a decrease in sintering shrinkage with the explanation that hydrogen was probably being trapped by lattice defects. This supposedly lowered the dislocation mobility and in turn their contribution to the sintering process [44]. Although a large difference in self-diffusion coefficients exists between volume and dislocation pipe diffusion, the effect is lost dramatically with only low levels of carbon content in the material [45].

15

Figure 8, redrawn from [46], summarizes the most relevant "rules of thumb" for diffusion in iron. There is a large difference in magnitude of the diffusion coefficients for substitutional and interstitial elements. Additionally, there is a strong dependence on the phase of the host lattice, i.e. if the iron exhibits the ferrite or austenite phase, with bcc or fcc crystal structure, respectively. The shift of diffusion coefficients on either side on the Curie point can possibly be utilized to determine whether or not a certain diffusion type contributes to sintering. A dramatic change in sintering shrinkage can indicate that volume diffusion is highly active, while a less noticeable difference would point towards grain boundary diffusion. This indicates that the purity levels of the metal plays a significant role when determining the role of diffusion along dislocations. It may be possible that any material system that harbours a number of impurities, such as a conventional water-atomized powder, will further act to decrease the dislocation pipe diffusion
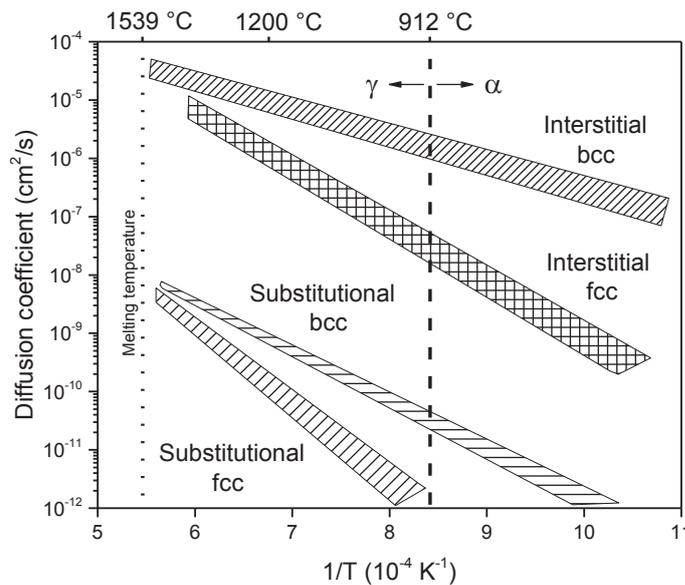

Figure 8: General overview of typical diffusion coefficients in iron. Redrawn from [46].

coefficient. If the powder analysed shows a tendency to have a surface enrichment of trace elements like Cr, Mn and Si, see paper I, then it is possible to imagine that the particle surfaces, when compacted together, form a sort of continuous grain boundary with segregated elements. This can possibly decrease the sintering contribution from grain boundary diffusion in favour of volume diffusion.

Sintering

Sintering, in essence, describes material movement taking place at temperatures below the melting temperature and is the key to most powder metallurgical processes. A large body of literature has dealt with sintering questions since its first description in the 1920's, with a large increase during recent years [17]. To understand, and to some degree predict, the sintering behaviour has been a huge incentive for the industries relying on sintering, with both energy and material savings being important.

Sintering is based on the activation of various diffusion mechanisms with the driving force being the minimization of surface energy [8]. While the movement of all atoms are important, sintering refers mainly to the self-diffusion of the base atoms. The mechanisms by which diffusion is possible are varied and act differently but can be summarized as surface diffusion, grain boundary diffusion, volume diffusion, plastic flow and evaporation/condensation.

Surface diffusion moves atoms from one surface location to another, but no shrinkage or densification is created in the process as the interparticle distance is not reduced [47]. Nonetheless, surface diffusion leads to sinter neck formation, which increases the strength of the compacts. Coarse powder compacts can e.g. show a negligible density increase whereas the strength increases dramatically. For carbonyl iron compacts, strength can remain constant even though density increases. Both cases point towards the influence of surface diffusion [18]. While surface diffusion can influence the strength of compacts, especially at relatively loose initial powder configurations, mechanical and other properties rely to a large extent on density. Densification requires densifying diffusion mechanisms where atoms move not from one surface to another, but are transferred to a sinter neck from inside the powder. Two of the most important diffusion mechanisms that are densifying are grain boundary and volume diffusion in which atoms move along grain boundaries or through the lattice, respectively. Plastic flow and evaporation/condensation are usually less important, but can play a role under certain conditions. Plastic flow is related to dislocations and can thus be significant for compacted powder. However, as dislocations are annealed out at elevated temperature, this mechanism loses importance. Evaporation/condensation is a type of surface transport mechanism and does not contribute to densification, but can influence sintering of low-stability materials like lead [8].

A common question regarding sintering is which types of diffusion mechanisms that are active at a given temperature. In general, it is seen that the diffusion coefficients of surface, boundary and volume diffusion follow the rule

$$D_S > D_{GB} > D_V \qquad (16)$$

However, they are affected differently by temperature, meaning that surface diffusion loses its importance with an increase in temperature [39]. Grain boundary diffusion typically has a lower activation energy than volume diffusion and consequently the energy input required is lower meaning that it will occur at lower temperatures [8]. However, the comparison between grain boundary and volume diffusion is typically normalized with respect to the available paths the diffusion species can take, i.e. the grain boundary diffusion coefficient is modified by the cross sections of the grain boundary to account for the limited area through which diffusion takes place [39]. The ratio between the sintering contributions of surface, grain boundary, and volume diffusion was indicated to change dramatically with powder size, and the role of densifying mechanisms relative to surface diffusion must be greater for fine powder to account for the shrinkage [47]. With reference to the general diffusion discussion above, sintering is also affected strongly by the phase of the material, something which has attracted attention [18,48]. Sintering of carbonyl iron has received interest due to its fine particle size, narrow size distribution and near spherical morphology [18].

The sintering and its kinetics can be assessed in multiple ways. Early experiments were e.g. concerned with understanding mechanisms of sintering through wire-spool and thermal grooving experiments [47,49]. Dynamic and isothermal sintering is often considered separately. Isothermal sintering kinetics are analysed by keeping the specimen at some elevated temperature and recording the evolution of some resulting properties of the sintering. Commonly, the dimensional changes or sintering neck diameter is considered. The kinetics are commonly associated with a power-law behaviour

$$\frac{\Delta l}{l_0} = Kt^n \qquad (17)$$

where $\Delta l/l_0$ is the sintering shrinkage, K is the compound factor describing the active diffusion mechanisms, t is the time at the isothermal hold, and n is the empirical exponent which depends on the mass transport mechanism; n = 0.33 for grain boundary diffusion and n = 0.4 for volume diffusion. K is given by

$$K_{gb} = \left(\frac{5\delta D_{gb}\gamma V_a}{kTD^4}\right)^{0.33} \qquad (18)$$

$$K_v = \left(\frac{2D_v\gamma V_a}{kTD^3}\right)^{0.4} \qquad (19)$$

where δ denotes the thickness of the grain boundary, γ denotes the surface energy, V_a is the atomic volume, k is Boltzmann's constant and D is the grain size. Plotting the results can give indications whether one diffusion mechanism is governing the shrinkage. Often, the results are mixed as the overall shrinkage is a combination of many active diffusion mechanisms. Nevertheless, this approach has found some success in model cases. The temperature sensitivity of the process can instead be extracted using dynamic methods. This can be done e.g. by analysing sintering curves and sintering rate peak positions and how these change with respect to a changing heating rate [50].

The sintering behaviour of other water-atomized powder grades has been investigated previously with a special reference to the sintering anisotropy [11,43,51–53]. Activation of the material, in terms of a defective interparticle contact region, is believed to enhance diffusion [43], although it is unclear what role recovery and recrystallization play as dislocations will be annealed out at some elevated temperature. The defective region is believed to originate from the compaction which introduces dislocations in the highly deformed areas. Low-angle grain boundaries, i.e. when two adjacent grains have low misorientation, can be described as an array of dislocations [54,55]. Consequently they can be linked to deformation.

A phase-controlling approach to sintering is also to some extent possible, utilizing the inherent effects of diffusion in response to a change in the crystallographic structure. The large drop in volume diffusion coefficients at the phase transformation can for example be delayed if bcc-stabilizing elements are added, such as molybdenum, phosphorous and silicon. If the iron matrix exhibits a ferrite phase to higher temperatures, more pronounced sintering can be achieved. Similarly, fcc-stabilizers such as nickel can hamper sintering [8].

While it has been discussed previously that suppressing surface diffusion can be beneficial so as to conserve the sintering driving force, comparisons between materials shown that this is not always the case. For carbonyl iron powder, a possible explanation for the increased density of samples heated at high rates is the inhibition of exaggerated grain growth [56].

Alternative sintering methods
The previous sections deals with solid-state sintering, i.e. the diffusion takes place in solids. By production volumes, it is the most commonly used sintering method. Liquid phase sintering, where one phase is brought above its melting temperature to facilitate sintering, is used in different material systems e.g. in the hard metal industry [57]. Rapid heating rates produced by alternative sintering routes such as microwave heating has been shown to exhibit higher density and hardness compared to conventional sintering for carbonyl iron powder, likely due to less microstructural coarsening. Additionally, the pore shape was rounder which improved mechanical properties [58].

Chapter IV – Materials and Experimental Methods

Materials

The materials used in this work were water-atomized iron powder, sieved to three different size fractions, and two carbonyl iron powder grades.

Water-atomized iron powder

Water-atomized iron powder is the workhorse of the conventional press and sinter route in the PM industry. The reason for this is mainly the low cost of the powder which allows for full utilization of the benefits of PM. Water-atomized powder is produced by means of atomization, in which a molten metal is let through a hole in a tundish in a vertical setup where the melt is disintegrated by streams of water. The atomization process parameters determine the subsequent properties of the powder, e.g. the mean size of the particles, the particle size distribution and the particle morphology. Additionally, the atomization affects the chemical properties of the powder as it introduces oxygen into the material. The oxygen levels are commonly reduced by introducing an annealing step before the subsequent processing.

The irregular particle morphology of water-atomized powder typically gives high green strength, i.e. after shaping operations, which allows for easier handling of the parts. This is a consequence of the metal particles being mechanically interlocked by protrusions.

The water-atomized iron powder used in this study was provided by Höganäs AB and is based on standard powder that was sieved into three different sieve fractions, <20 µm, <45 µm and <75 µm. It should be noted that the coarse powder fraction thus includes the finer fractions to some extent, with the particle size distribution shifted accordingly. These fractions will be referred to Fe20, Fe45 and Fe75 for the remainder of the thesis. The chemical composition of the three powder fractions can be seen in Table 1.

Table 1: Chemical composition of the three powder fractions.

Powder	Chemical composition (wt.-%)								
	C	N	O	S	Mn	Cr	Si	Sn	Fe
Fe -20 µm	0.0065	-	0.155	0.0093	0.100	0.060	0.007	0.002	bal.
Fe -45 µm	0.0048	-	0.114	0.0093	0.087	0.056	0.004	0.003	bal.
Fe -75 µm	0.0058	-	0.105	0.0085	0.084	0.047	0.003	0.003	bal.

Based on this, it is clear that the powder is rather clean with only some minor impurity elements in addition to the iron. Oxygen naturally reacts with the iron to form a thin iron oxide layer covering all powder particles. The layer contains the about half of all oxygen in the powder, depending on particle size, with a large fraction of the rest being locked as iron oxide inclusions in the matrix or at grain boundaries. Some oxygen is also found as part of thermodynamically stable oxides, mostly confined to the surface. Iron of all phases has low solubility of oxygen [59], and thus only a small amount can be dissolved in the matrix. The small differences that exist between the powder size fractions are due to the increasingly larger surface area of the finer fractions, which influences the content of impurity elements and oxygen. An overview image of the Fe45 powder can be seen in Figure 9a.

Carbonyl iron powder

Two carbonyl iron powder grades commonly used in MIM were obtained from BASF SE. One grade is the standard MIM grade designated OM, while the other grade is the hydrogen annealed grade designated CC.

In contrast to most other types of metal powder used in the PM industry, carbonyl iron powder is not atomized. Instead, it is produced via a special thermochemical decomposition process, the carbonyl process, invented and commercialized by BASF in 1925. Iron powder is reacted with carbon monoxide to form a gaseous metal-organic complex, the carbonyl complex, which is subsequently condensed by adjusting the pressure and lowering the temperature [26]. The resulting powder contains particles that are much finer than
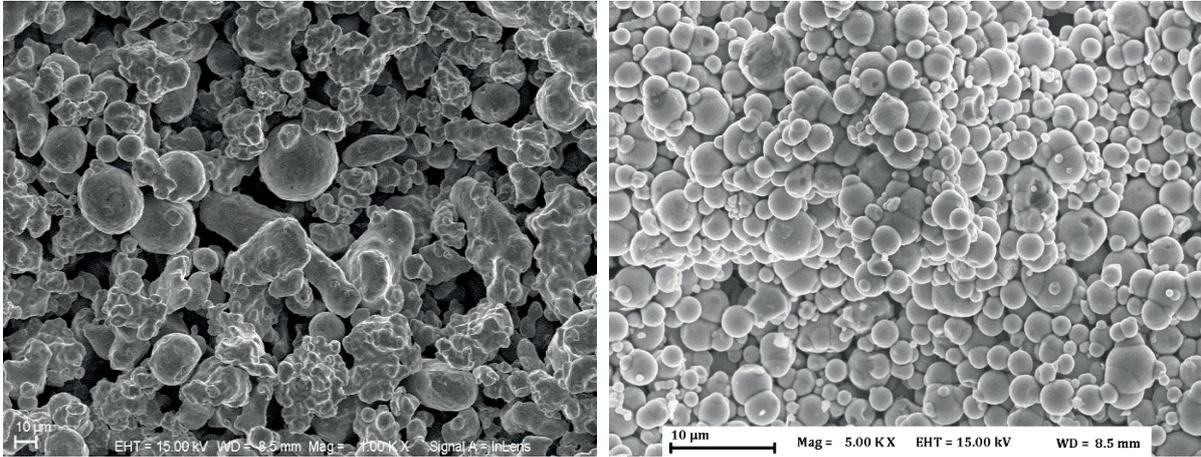

Figure 9: Overview of the a) Fe45 powder, and b) carbonyl iron powder grade OM. Note that the carbonyl iron particles are considerably finer.

in a regular atomized powder, d_{50} = ~5 μm, along with a more narrow particle size distribution and highly spherical morphology, see Figure 9b. This combination of physical properties makes the carbonyl powder ideal for metal injection moulding purposes allowing for a very high sintering driving force and mouldability. However, one drawback is the high cost of the powder. The chemical composition of the carbonyl iron powder grades can be seen in Table 2.

Table 2: Chemical composition of the two carbonyl iron grades.

Powder	Chemical composition (wt.-%)						
	C	N	O	S	Cr	Si	Fe
Carbonyl OM	0.795	0.75	0.2689	0.0022	<0.001	0.003	bal.
Carbonyl CC	0.016	0.00633	0.2582	0.0017	<0.001	0.05	bal.

It should also be noted that carbonyl iron grades are typically classified as hard or soft, depending on their chemical composition, with hard grades containing carbon and nitrogen and soft grades being plain iron. The crystal structure of the hard grades are commonly described as a layered onion-structure, with nano-crystalline carbide and nitride phases like Fe_3N, Fe_4N and Fe_3C. These comprise the major fraction of the alloying elements. In a hydrogen atmosphere, there is a gradual transition from hard to soft powder as the carbides and nitrides are reduced [60].

Sample preparation: Uniaxial die-compaction, metal injection moulding, delubrication and debinding

For experiments, the powder was either used in an as-received condition or subsequently pre-processed according to its designated production route, i.e. the water-atomized iron powder was mixed with a lubricant and uniaxially die-compacted, whereas the carbonyl iron powder was mixed with a binder and injection moulded. Both die-compaction and metal injection moulding were done at Höganäs AB.

For die-compaction performed at Höganäs AB, the water-atomized iron powder was mixed with 0.6 wt.-% LubE for lubrication. Graphite was also admixed for some of the powder mixes to provide a carbon source. The compaction was done using three different compaction pressures. Cylindrical samples were produced, 11.3 mm in diameter and 13.5-14.7 mm in length, depending on the applied pressure. The resulting compressibility curves are shown in Figure 10.
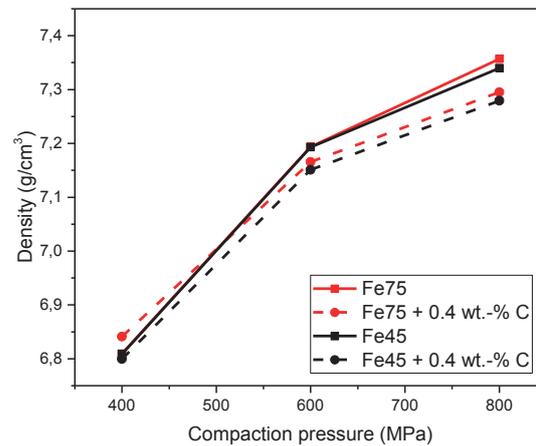

Figure 10: Compaction curves for the four different mixes of water-atomized iron powder.

Injection moulding was performed at Höganäs AB with a proprietary binder system using a Battenfeld 400-130 instrument. The solids loading was set to 54 vol.-%.

A tube furnace was used for the bulk of the delubrication experiments as well as for the thermal debinding of the injection moulded samples. Green samples were loaded onto alumina crucibles and inserted into a quartz tube. The temperature was ramped to 450 °C with a heating rate of 10 °C/min. Argon was flowing at 4 l/min to minimize oxidation. It should be noted that any oxygen pickup was deemed to be of relatively low importance due to the subsequent sintering in hydrogen. Thermogravimetric experiments performed on compacts was affected nonetheless.

Experimental methods
Several different experimental methods were used in this thesis with special emphasis on thermoanalytical and surface analytical techniques.

Thermoanalytical techniques

Thermogravimetric analysis
Thermogravimetric analysis (TGA) is a thermoanalytical measurement technique used to record the mass changes of a specimen to a very high degree of accuracy. Despite its relatively simple principles, TGA is a powerful method capable of giving information of dehydration, oxidation, reduction etc., given a set temperature profile. An integral part of the function of the thermogravimetric equipment is its combination with atmosphere control that allows for well-defined experimental setups.

The instrument used for all thermogravimetric work was a simultaneous TGA/DTA/DSC thermal analyser STA 449 F1 Jupiter from Netzsch. Experiments were done in a high temperature SiC tube furnace with a

W-Re thermocouple for monitoring the temperature. The sample masses were typically around 2 g and they were loaded into a large Al_2O_3 crucible. The instrument was flushed with high-purity argon (99.9999 % purity) three times before each measurement.

The experiments were run in either pure argon or pure hydrogen (same purity as above). The temperature span was between 800 and 1350 °C, with holding times of 30-60 minutes. For the kinetic analyses, the heating rates were varied between 1 and 50 K/min.

Differential scanning calorimetry
Differential scanning calorimetry (DSC) is thermoanalytical technique employed to record the heat flow difference between the sample investigated and a reference. Because of this, the requirement is that the analysed event is either endothermic or exothermic, i.e. heat is either taken up or released by the sample. Processes that can be recorded include phase transformations, chemical reactions, decompositions, and even magnetic transitions such as the Curie point.

The instrument used for the DSC measurements was identical to the TGA equipment but was equipped with an S-type DSC sensor to allow for simultaneous measurements of TG and DSC signals. The sample masses were typically 100-250 mg, loaded into small Al_2O_3 crucibles.

The experiments were run in high purity argon (same purity as above) up to 1350 °C with a holding time of 30 minutes and using a heating and cooling rate of 10 K/min.

Dilatometry and quench dilatometry
Dilatometry is a thermoanalytic method utilized to investigate the dimensional changes of a specimen when it is subjected to a specific temperature program. A push-rod is coupled to a sensitive length calibration cell which gives a continuous reading of its position. When placed near a sample and a small force is applied, the linear dimensional change of the sample is recorded. The instrument is capable of recording the changes with high accuracy. Because of this, the dilatometer is widely used in the PM industry as it offers an excellent way of characterizing materials during sintering. Most phase transformations, e.g. the ferrite-austenite transformation, are associated with a change in dimensions, and consequently, the onset and stop of these transformations can be recorded with a dilatometer.

The instrument used for the dilatometer measurements was a DIL 402 C from Netzsch.

A quench dilatometer was used to complement conventional dilatometry instrument in various heat treatment situations where high heating or cooling rates are required. The quench dilatometer has an induction heating system which heats the material through Joule heating. Heating rates of 5 °C/s were used, with a cooling rate of ~30 °C/s.

The capabilities of the thermoanalytical techniques are summarized in Table 3.

Table 3: Measurement capabilities of the thermoanalytical techniques.

Technique	Mass	Phase transformations	Chemical reactions	Atmosphere control	Dimensional change
Thermogravimetric analysis	X		Yes, if mass change	X	
Differential scanning calorimetry	X	X	X	X	
Dilatometry		Yes, if dimensional change		X	X

Surface analytical techniques

X-ray photoelectron spectroscopy

X-ray photoelectron spectroscopy (XPS), also known as electron spectroscopy for chemical analysis (ESCA), is a surface sensitive technique that records the characteristic photoelectrons generated by monochromatic X-rays directed onto the sample. Since the emitted photoelectrons will have slightly different binding energies depending on their chemical state, the XPS analyses will provide detailed information about the surface chemistry of the material. The XPS is a surface sensitive technique and the escaping photoelectrons can only emerge from the outermost surface of the analysed sample, i.e. from about 1-10 nm.

In this study, the surface chemical state of both water-atomized and carbonyl iron powder was analysed using a PHI 5500 instrument equipped with a monochromatic Al Kα (1486.6 eV) X-ray source for the photoelectron generation. Powder samples, i.e. all samples that were neither compacted nor sintered, were mounted on a carbon tape for the analysis. The analysed area was around 0.8 mm in diameter for the chosen aperture size, meaning that a representative number of metal particles were analysed [23]. A pass energy of 23.5 eV with a step size of 0.1 eV was used for the detailed high-energy spectra.

Analysis and curve fitting was done using the software PHI Multipak using asymmetric curves and a Shirley background. Depth profiling was performed by etching with Ar^+ ion beam rastered over the analysis area yielding an etch rate of approximately 3 nm per minute. The etch rate was calibrated on a flat tantalum foil with 100 nm Ta_2O_5 oxide thickness. The etch depths thus refers to units of ion etching of Ta_2O_5. Nonetheless, the etch rates are assumed to be in reasonable agreement with etching of iron oxide [23].

Auger electron spectroscopy

Auger electron spectroscopy (AES) is a surface analytical technique that detects Auger electrons emitted from the material. The interaction volume in this technique is relatively small; the use of a focused electron beam together with the surface sensitivity means that the Auger signal can be recorded for a small area around 10 nm and typically originates from 1-10 nm below the surface. Consequently, accurate measurements of surface chemical composition of small features can be performed. The sensitivity and analytical spatial resolution is also combined with secondary electron imaging, allowing for both imaging and analysis of small surface features. Here a scanning PHI 700 instrument was used, with an accelerating voltage of 10 kV and a beam current of 10 nA.

A number of previous studies have utilized AES for depth profiling and surface analysis in various metal powder systems [5,23,61,62]. However, it should be noted that AES is only semi-quantitative in nature due to difficulties in assessing the peak intensities and their relation to chemical composition.

Scanning electron microscopy

Scanning electron microscopy (SEM) offers excellent information about the microstructural features of a material. Very high magnifications and spatial resolutions can be realized, providing surface topographical details by means of the secondary electron detector or elemental information using the back-scatter electron detector. One of the main strengths of the technique is its versatility and synergistic effects with e.g. energy dispersive X-ray analysis (EDX) and electron back-scatter diffraction (EBSD). However, microstructural investigations of highly ductile materials, such as plain iron powder, can be difficult as smearing of the material can cause superficial pores to close, giving inaccurate information when the density is cross-referenced with water-displacement methods [63]. The instrument used was a LEO Gemini 1500 FEG-SEM coupled with an XMAX analyser. Acceleration voltages of 15 kV were used with an In-lens detector, with a working distance of around 8.5 mm.

Energy dispersive X-ray analysis

The EDX can give qualitative chemical information about the surface and any features on it. The limitations are imposed by the large interaction volume of the electron beam with the sample. Thus it is not an ideal technique when analysing the chemical nature of small particulate features on powder surfaces.

Electron back-scatter diffraction

Electron back-scatter diffraction (EBSD) allows for collection of crystallographic information, including e.g. the crystal structure of a grain and its orientation and texture. In this study, EBSD was used for determining misorientation recorded from adjacent pixels to create a map of the misorientations across the analysed sample surface. The maps, which can span across particle cross sections can then be used to determine the prevalence of grain boundaries with a defined angle. By setting the map angle threshold to values commonly used to define low- and high angle grain boundaries, the location and density of such boundaries can be identified [55]. Low angle grain boundaries were defined as when the misorientation angle was between 2 and 10°, whereas high angle grain boundaries were set to be at a misorientation angle > 10°. The EBSD maps used were acquired with a Nordlys II detector (Oxford Instruments). The acceleration voltage was 20 kV with a working distance of 15-20 mm. The step size was varied between 0.1 and 2 µm depending on the features to be analysed. All generated maps were processed using the Channel 5 software.

Chapter V – Main Results and Summary of Appended Papers

The results and summary section is a compilation of the work done for the appended papers and will be divided into three main parts. The first part covers the surface analysis of powder of all grades, the second part deals with thermogravimetric analysis and kinetics while the last part summarizes the sintering studies. Both the fine water-atomized and carbonyl iron powder are discussed.

Surface characteristics of water-atomized iron powder

The surface characteristics of three water-atomized powder grades were studied in paper I and serve as a baseline for the subsequent analyses and sintering trials. A number of previous studies in the field [5,6,23,24] have established a methodology of powder analysis that is applicable to a wide range of powder grades used in classical PM. A great deal of the powder analysis has been conducted on water-atomized iron powder pre-alloyed with e.g. Cr and Mn that is widely used in the PM industry. For thermodynamic reasons, detailed in Chapter III, these elements are highly susceptible to oxidation compared to the iron matrix.

The methodology developed previously is expanded and applied to one of the workhorses of the powder metallurgy industry, i.e. plain water-atomized powder with relatively low level of impurities, see Table 1 in Chapter IV. Being nominally near-free of elements other than iron, the plain water-atomized iron powder is a seemingly simple material system although, as indicated in Chapter III, this is not the case. Despite the low level of impurity elements such as chromium, manganese and silicon, their thermodynamic tendencies to form oxides that are more stable than iron oxides cause an alteration of the surface and bulk chemistries of the powder. This can in turn have consequences for the subsequent sintering outcome. Additionally, studies have also indicated the effect of impurities on various types of diffusion.

X-ray photoelectron spectroscopy results, partly shown in Figure 11, indicate a surface enrichment of the impurity elements for three powder fractions. Furthermore, there appears to be a strong particle size dependency on the enrichment where fine particles tend to have more impurity oxides on their surfaces. Manganese and silicon show the highest enrichment, while there is no clear trend for chromium. The intensities of the metallic iron peaks relative to the peak intensity at the maximum etching depth of 50 nm can be seen in Figure 11c. With the basis in a model, the thickness of the surface iron oxide layer was estimated to be 6-7 nm. No large difference between the three powder fractions was found, but the finer powder fraction was nevertheless analysed to show slightly thicker oxide layer.

When viewing the surface chemical composition of the Fe45 powder fraction, it is seen that most signals representing elements on the surface are decreased with an increase in etch depth. The iron signal increases with increasing etch depth as removal of material means that the material becomes closer and closer to its nominal composition. Once again, the enrichment of the impurity elements in cation states can be seen.
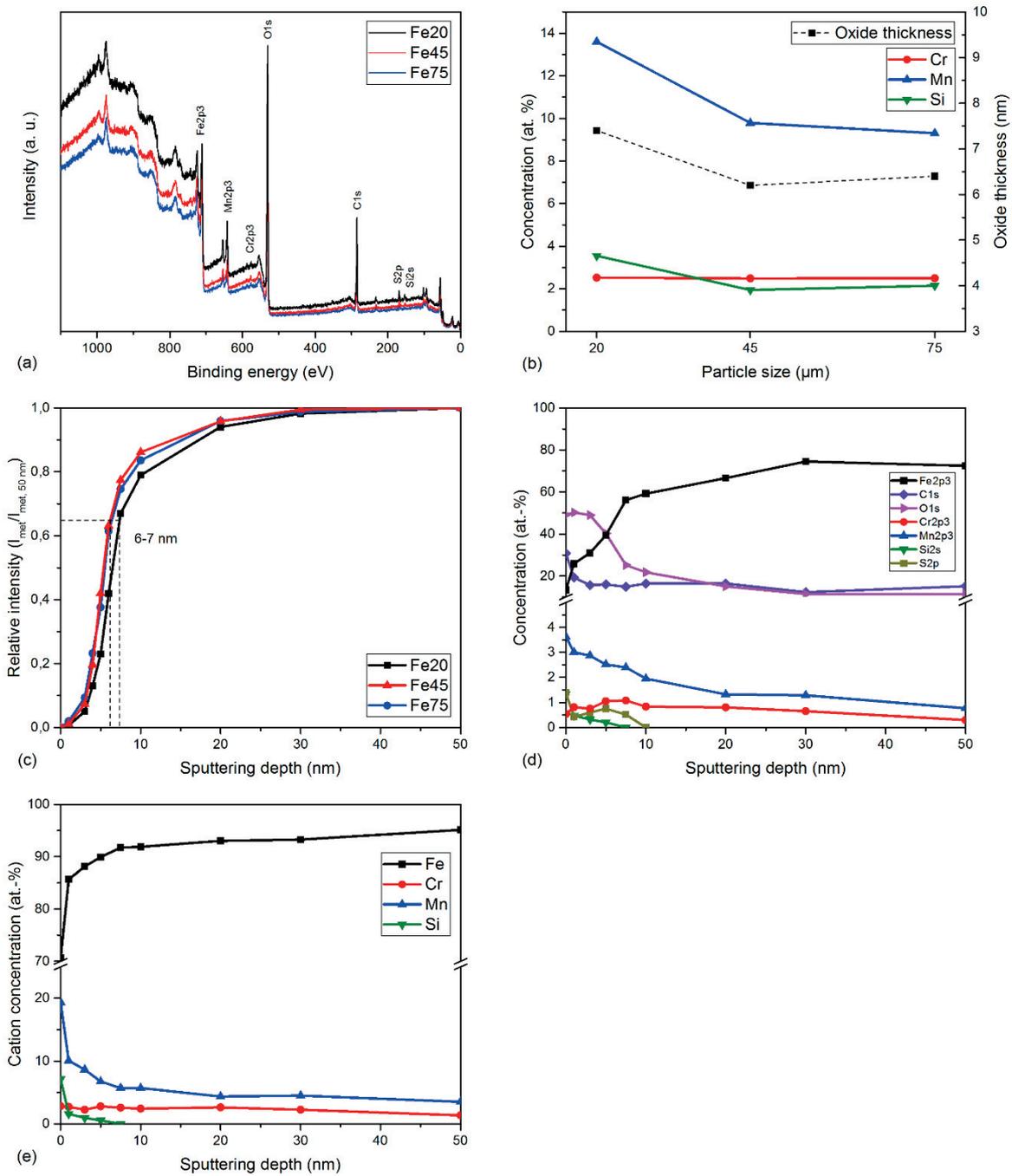
Figure 11: XPS results detailing the surface chemical state of three powder fractions. From paper I.
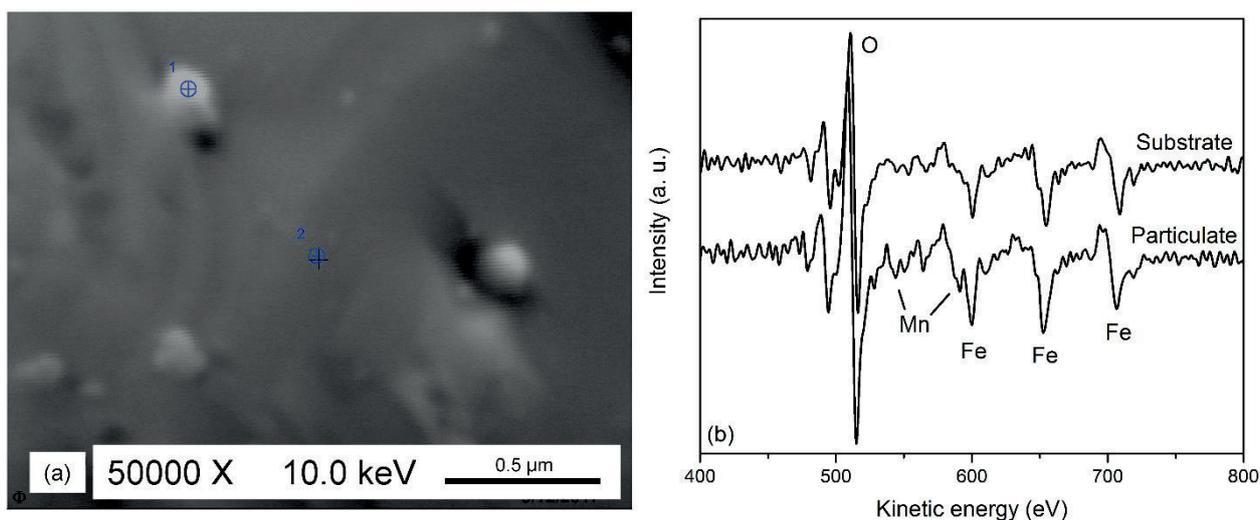
Figure 12: AES analysis providing information about the surface chemical state difference between a surface feature that is a particulate oxide, and the surrounding powder particle surface.

The AES was used as a complement to the XPS analysis to provide excellent spatial resolution combined with spectroscopic point analysis. Figure 12a shows a detailed view of the surface of a particle of the Fe45 powder along with particulate features. The corresponding AES spectra in Figure 12b indicate that the particulate is enriched with manganese. The substrate itself does not contain any significant amounts of manganese but only iron and oxygen which is characteristic of the surface iron oxide layer. It should be noted that in order to detect the presence of Mn, the content must be significant due to overlap with Fe peaks that would otherwise hide the Mn signal.

Thermogravimetric analysis of water-atomized and carbonyl iron powder

Thermogravimetric analysis is an invaluable tool for studies of the thermal stability of a material. Along with a very precise control of the temperature and atmosphere of the experiment, the mass changes can be recorded accurately. Figure 13 shows the thermogravimetric curves for three different powder fractions of the water-atomized iron powder, see paper I.

Two different regions of the curves can be identified, first related to the iron oxide layer reduction and then to oxygen diffusion and removal at elevated temperatures. The first dramatic change with a mass loss at around 400 °C is due to the reduction of the surface iron oxide layer by hydrogen. Corroboration by analysis of X-ray photoelectron spectroscopy results, that indicated that the surface oxide layer thickness was roughly similar for the three powder fractions, reveal that the initial mass loss only depends on the effective surface area of the powder. By this relationship, it is possible to get a reasonable estimate and a validation of the surface iron oxide layer thickness of the powder particles by performing a series of thermogravimetric experiments if the surface area is also known. The following relationship was established

$$m_{TG(g^{-1})} = t_{oxide} \cdot BET \cdot \rho_{oxide} \cdot 0.3 \qquad (20)$$

where $m_{TG(g-1)}$ denotes the mass lost per gram of initial mass as recorded by thermogravimetric analysis, t_{oxide} is the thickness of the oxide, the BET-value is a measure of the surface area per unit of mass acquired from gas adsorption, ρ is the density of the oxide and 0.3 is the mass fraction of oxygen in the Fe_2O_3 oxide. Note that this value will vary depending on the chemical composition of the oxide. In this case, the majority of the oxide will be Fe_2O_3 which is taken as the base for the calculations. XPS curve fitting distinguishes between the oxidation states but this is not considered further for the thermogravimetric measurements.

27

The difference in the magnitude of the initial mass loss is connected to the particle size distribution in the powder, reflecting the number of small particles in a given sample. As smaller particles have larger surface
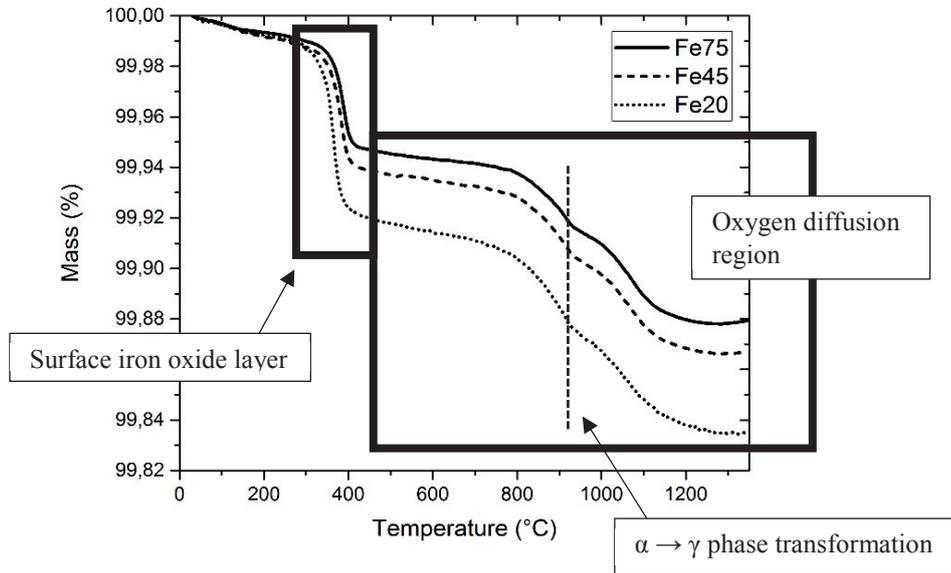

Figure 13: Thermogravimetric curves of three powder fractions. From paper I.

area to volume ratio, the total effective specific surface area of fine powder will be much larger than for coarse powder. Consequently, more oxygen is bound to the surface and in turn, more oxygen is available for removal by hydrogen during the reduction process. A particle size dependence where finer particles are reduced at lower temperatures may be present but was not analysed further. It is likely that a similar procedure can be followed to study the reduction of thermodynamically stable oxides, but this requires that they are present in a significant amount.

Oxygen diffusion in iron powder

Beyond the initial mass loss of the typical thermogravimetric curve there is a region of relatively stable mass of the powder sample. At this point, the surface iron oxide layer is completely removed, leaving a surface of metallic iron separating particulate oxide islands. This unbalances the composition profile of oxygen in the metal particles and leads to outwards diffusion of oxygen. As the solubility of oxygen is low in either of the iron phases [59], the oxygen is likely bound as internal oxides in the bulk or at grain boundaries. However, there will be a drive for the oxygen to leave the insides of the powder particles because of the continuous removal of oxygen by hydrogen that takes place on the surface. This is valid only when all impurity elements forming thermodynamically stable oxides are saturated with oxygen and the oxygen transfer mechanisms become inactive. The movement of oxygen out of the iron matrix is relatively slow at low temperatures but dramatically accelerates at elevated temperatures owing to the Arrhenius relationship governing diffusion. With reference to the diffusion theory outlined in Chapter III, the oxygen movement is also dependent on the current phase of the material, i.e. whether the iron matrix exhibits the bcc or fcc crystal structure, which explains the twist in the curve at the phase transformation temperature in Figure 13. There is thus a large effect on diffusion due to the change in crystal structure which causes the rapid oxygen diffusion at the end of the ferrite region to slow down considerably after the transformation to austenite. This is illustrated in Figure 14 where two powder samples were brought to 900 and 920 °C, respectively, and held for one hour in pure hydrogen. The resulting mass loss corresponds to oxygen atoms being reacted with hydrogen on the surface and the phase dependence of the diffusion process leading to this stage. The

diminishing rate of mass loss is a consequence of the change of the compositional profile of the powder particles, with a gradual depletion of oxygen from oxides at increasing depths as the diffusion proceeds. Consequently, a particle size dependence should be present which reflects the difference in diffusion lengths. This is something that was briefly noted previously for the case of carbothermal reduction mechanisms [3].
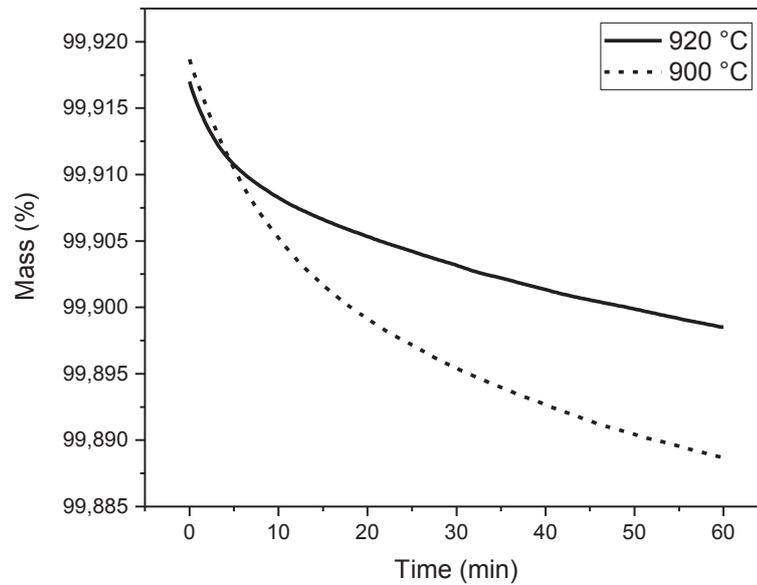

Figure 14: Mass loss due to oxygen diffusion. Depending on the current phase of the host matrix, the interstitial diffusion proceeds at different rates.

Kinetic analysis of water-atomized and carbonyl iron powder

The importance of the surface iron oxide layer and the diffusion of oxygen calls for even more in-depth analysis. For this reason, the kinetics of iron oxide reduction and the subsequent outwards oxygen diffusion in a hydrogen atmosphere were studied. With reference to Chapter III where the basics of kinetics were outlined, processes where mass is lost at elevated temperatures can be studied based on Kissinger's formulation [33,34]. The analysis yields the activation energy associated with the mass loss processes which can be used to describe e.g. how the reduction proceeds at arbitrary sintering temperatures which may be important in determining the extent of oxygen free interparticle contacts during the initial stages of sintering.

The details of the analysis of the water-atomized iron powder grades can be seen in Figure 15 from paper II where a number of thermogravimetric curves and their corresponding derivatives are plotted for the respective powder fractions of Fe20, Fe45 and Fe75. Three distinct peaks can be seen in all derivative curves. The first one corresponds to the reduction of the surface iron oxide layer. The two following ones
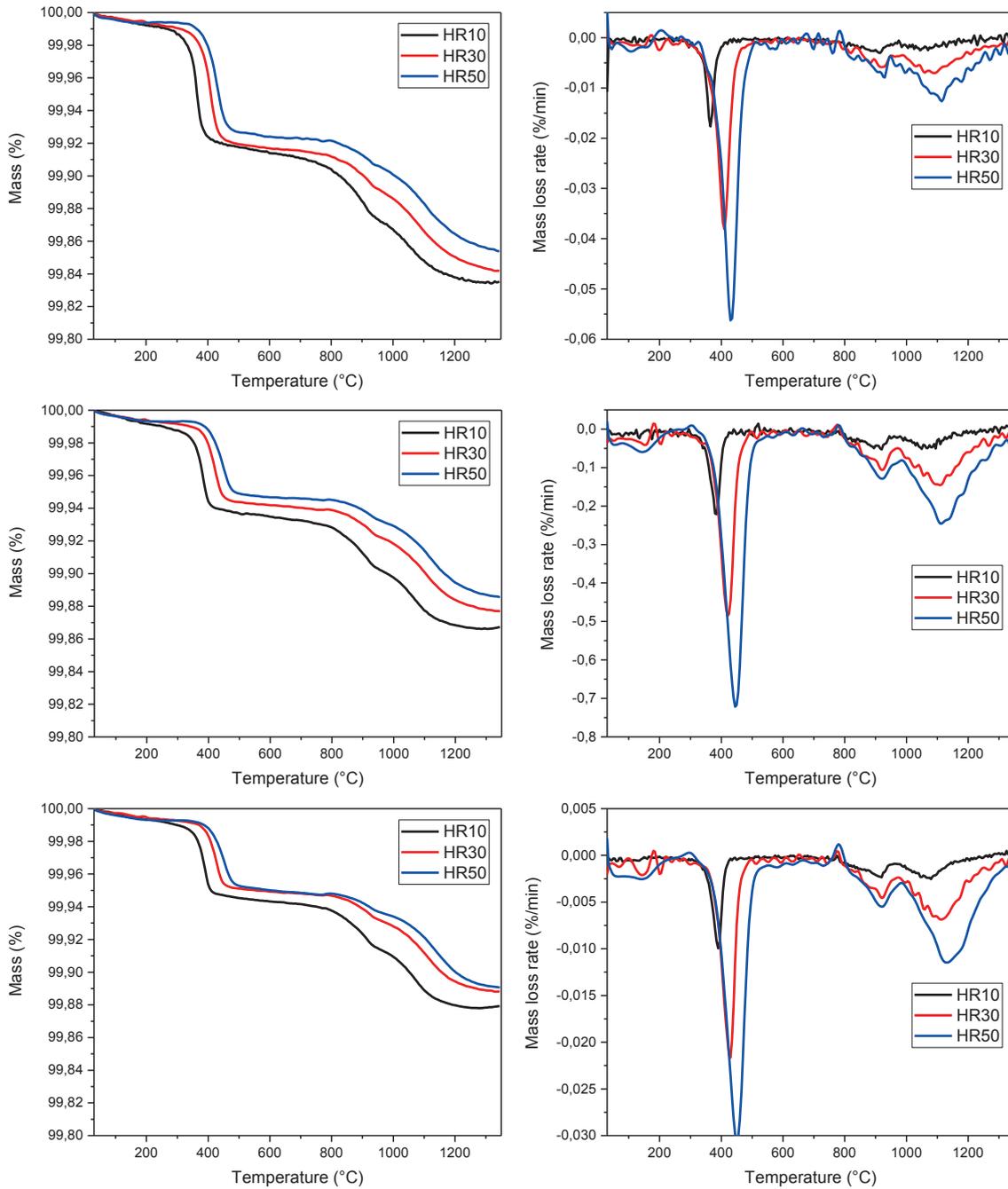

Figure 15: Thermogravimetric curves of water-atomized iron powder used for the kinetic analysis of the iron oxide layer. Fe20, Fe45 and Fe75 in pairs from top to bottom.

instead reflect the mass lost by outwards diffusion of oxygen and subsequent reduction. The position of the first peak, and the lack of temperature shift at increasing heating rates, indicates that this mass loss is

30

connected to the rapid outwards diffusion in the end of the ferrite region. The rate of mass loss thus peaks just before the transformation temperature is reached, where diffusion is slowed down. The reason is that oxygen diffusion is heavily affected by the crystal structure of the iron. Above the transformation, the diffusion rate is slightly delayed because of the austenitic fcc phase before it will again lead to a large mass loss. There is also a clear shift in the peak temperature position with heating rate, qualifying it for a kinetic analysis. The peak positions corresponding to oxide layer reduction and oxygen diffusion were extracted from the derivative curves in Figure 15. The corresponding kinetic plots are shown in Figure 16a, with the fitting details available in paper II.

The activation energies for the surface iron oxide reduction were determined to be 81, 87 and 95 kJ/mol for Fe20, Fe45 and Fe75, respectively. The values are in the same order of magnitude as previously studied reduction of iron oxide [35,38,64]. For the high-temperature mass loss related to diffusion, the activation
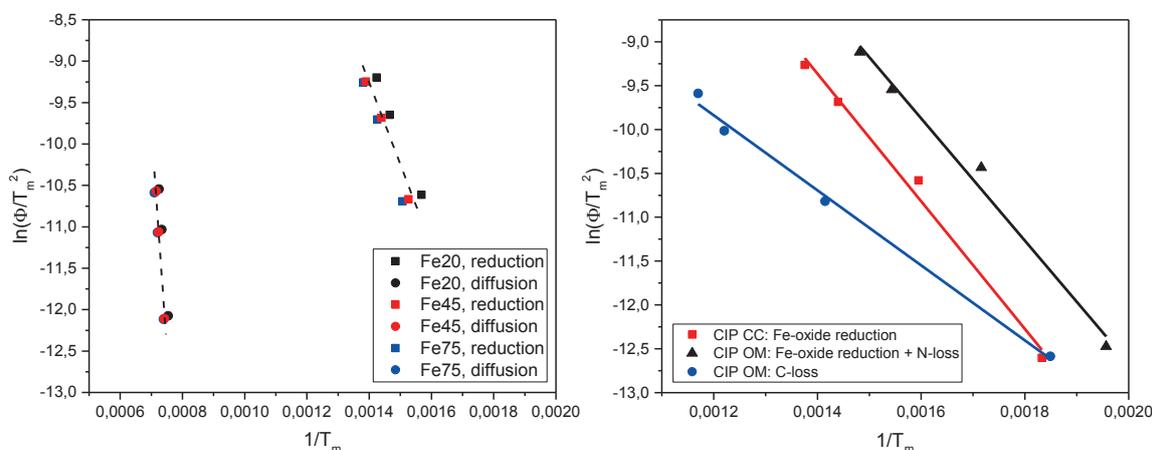

Figure 16: Kinetic plots for a) water-atomized and b) carbonyl iron powder.

energy was found to be 432, 489 and 436 kJ/mol for Fe20, Fe45 and Fe75, respectively. This is significantly higher than acquired from oxide reduction, but the reason may be that this thermogravimetric method only indirectly reflects the diffusion of oxygen and the subsequent reduction, as opposed to e.g. radioactive tracer methods. Thus it may not represent a single distinct activation energy, but rather a compound activation energy related to the decomposition of internal oxides, oxygen diffusion, and subsequent reduction. However, with reference to the activation energies of the oxide reduction, this is likely not the limiting step. Although not discussed here, the reduction steps could be evaluated further if coupled with XPS to determine the oxide structure on a detailed level. A similar approach was used in the present discussion, no such evaluation was done on the oxide layers [25]. If combined with a kinetic analysis, these results can maybe yield more accurate results of how the structure and kinetics of reduction work in conjunction during the present conditions.

A similar thermogravimetric study was done in paper III on carbonyl iron powder where the hydrogen annealed grade exhibits a reduction behaviour very similar to the water-atomized iron powder. The standard OM grade contains nitrogen as well as carbon and consequently behaves differently. The corresponding kinetic plots are shown in Figure 16b, with the fitting parameters presented in paper III.

The activation energies were determined to be 59 kJ/mol for grade CC as well as 58 and 35 kJ/mol for the first and second peaks of grade OM, respectively. The values are in reasonable agreement with values reported previously for reduction of iron oxide, especially for magnetite reduction [35]. The activation

energy of nitrogen removal could not be separated from the values of iron oxide reduction in the current analysis, and they are believed to be similar. The break-up of carbide phases of carbonyl iron was studied elsewhere, but no kinetic analysis of this degradation was done [60]. Compared with water-atomized iron powder, a size dependence can be seen with the significantly finer carbonyl powder grades being reduced at lower temperatures. Additionally, the composition of the standard grade with high contents of nitrogen and carbon may influence the onset and peak temperatures of the oxide reduction, affecting its kinetics.

Sintering behaviour of compacted water-atomized iron powder

Apart from the surface characteristics and the reduction behaviour at elevated temperatures, the sintering outcome depends strongly on the initial conditions of the green compacts. Shaping powder through compaction will inevitably lead to particle rearrangement and with higher compaction pressures, plastic deformation. Uniaxial die-compaction also leads to anisotropic green density gradients where regions parallel to the compaction direction are more heavily deformed than regions transverse to the compaction direction.
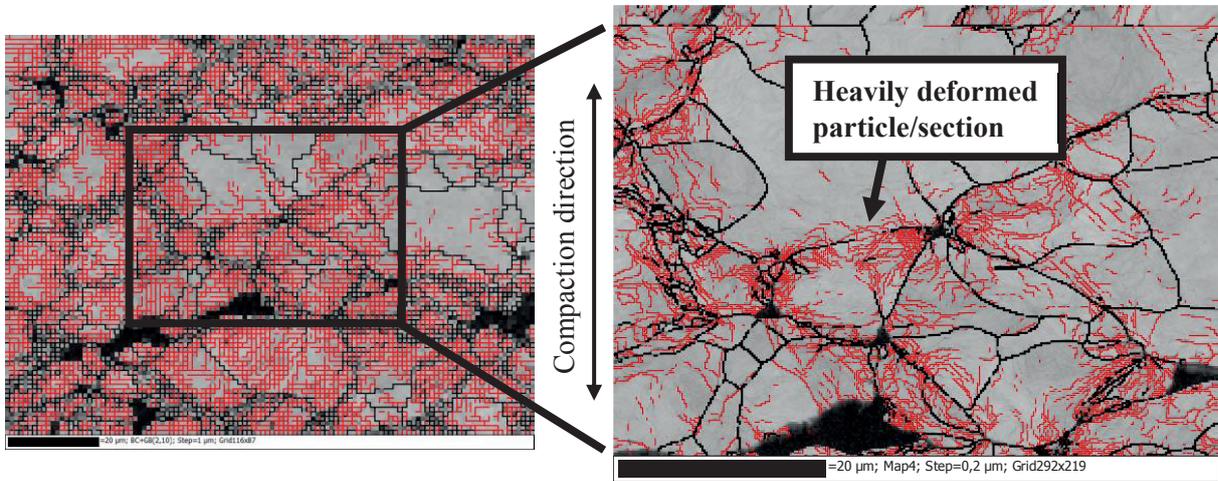

Figure 17: EBSD maps of green compacts of Fe75 + C, compacted at 800 MPa with low- and high-angle grain boundaries depicted in red and black, respectively.

As explained in paper II, the deformation taking place will likely be localized to mainly interparticle contact regions or smaller sections or protrusions of the highly irregular powder particles, see Figure 17. The bulk of the particles will remain undeformed as long as pores and protrusions are more easily compacted. As a result of the compaction, interparticle regions will be flattened which increases the effective contact area between the particles. This in turn causes an enhancement of the initial sinter neck formation, facilitating a shrinkage in the ferrite region.

An attempt was done to use differential scanning calorimetry (DSC) to study the stored energy of compacted samples, which when heated will trigger recovery and recrystallization and a corresponding release of energy due to exothermic nature of the processes. It is thought that recrystallization starts at around 0.5 of the homologous temperature T/T_m which is around 450 °C for pure iron [65,66]. One problem with these measurements is the relatively small amount of energy released during recovery and recrystallization. Other issues include masking of the signal by oxidation and very careful preparation is needed [66]. The experiments did show some promise, but is likely capturing events related to sintering.

Sintering was performed with number of samples of different green densities with a variety of experimental setups. Both low- and high-temperature sintering trials were done to capture the behaviour. The results can partly be seen in Figure 18. Isothermal sintering experiments show an increase in shrinkage with

temperature, as expected. The difference in initial compaction and its effect on sintering will be visible at 700 °C with an increasing deviation at higher temperatures. The main contribution was attributed to changes in initial interparticle contact flattening, with possible enhancement from altered diffusion due to dislocations. As a consequence, the shrinkage will not follow the classical power laws that can be used to describe sintering.
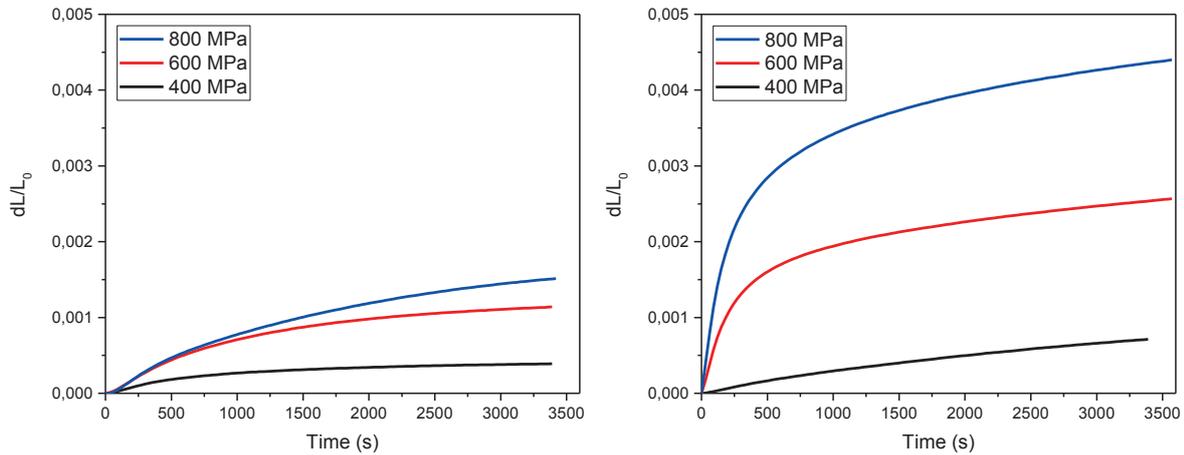

Figure 18: Low temperature sintering of water-atomized iron powder, a) 700 °C, b) 800 °C.

Fracture surfaces were acquired from the compacts sintered at low temperatures to track the evolution of the microstructure in terms of e.g. sinter neck formation, see Figure 19. A small amount of necks can be
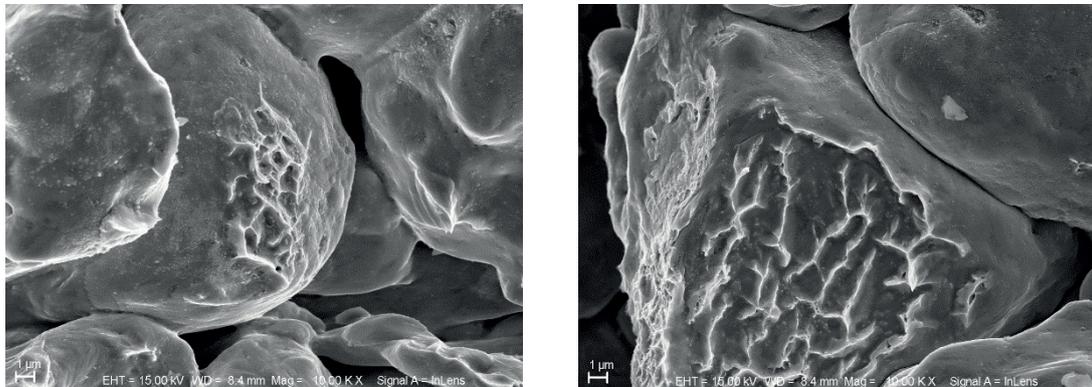

Figure 19: Fracture surfaces of compacts sintered at 700 °C, a) 400 MPa, b) 800 MPa.

recorded at the low sintering temperatures with an increase at elevated temperatures as expected. For the samples compacted at 400 MPa, the low amount of shrinkage recorded by dilatometry points toward the importance of surface diffusion with only a minor contribution from the densifying diffusion mechanisms.

Several sintering experiments were conducted at higher sintering temperatures of 1350 °C while also exploring the effect of varying parameters like the heating rate, particle size, compaction pressure and carbon content. The results, see paper II, further indicate the importance of the compaction pressure in the high-diffusivity ferrite region. It is also seen that samples with the lowest green density exhibits the largest shrinkages at high temperatures, likely a consequence of the open compact structure that did not sinter at low temperatures. The heating rate effectively controls the time spent in each phase region which

subsequently determines, at least partly, the total sintering shrinkage and density. Some results can be seen in Figure 20.
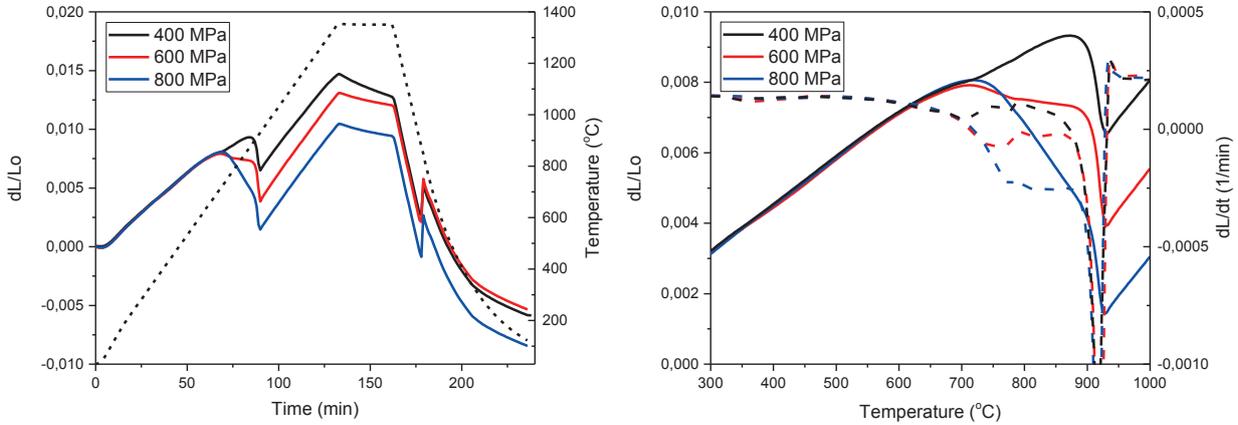

Figure 20: Sintering of Fe75 at 10 °C/min for three compaction pressures. a) Full sintering cycle, b) detailed view.

Sintering behaviour of carbonyl iron powder

Sintering of the carbonyl iron compacts was conducted in similar fashion, see paper III. An example is shown in Figure 21 for both the standard OM and annealed CC grades. The sintering is strongly affected by the heating rate for both grades. Sintering proceeds with rapid sintering in the ferrite region along with slower densification when transitioning into the austenite region. The shrinkage at the isothermal sintering temperature of 1350 °C is largely a function of the time spent during the heating stage and is affected by the ferrite-austenite transformation. For the carbon-containing OM grade, the heating rate governs whether or not carbon is being removed during the heating stage. With a slow heating rate, carbon is removed whereas with a fast heating rate, carbon is kept until the transformation where it is dissolved in the austenite. For the
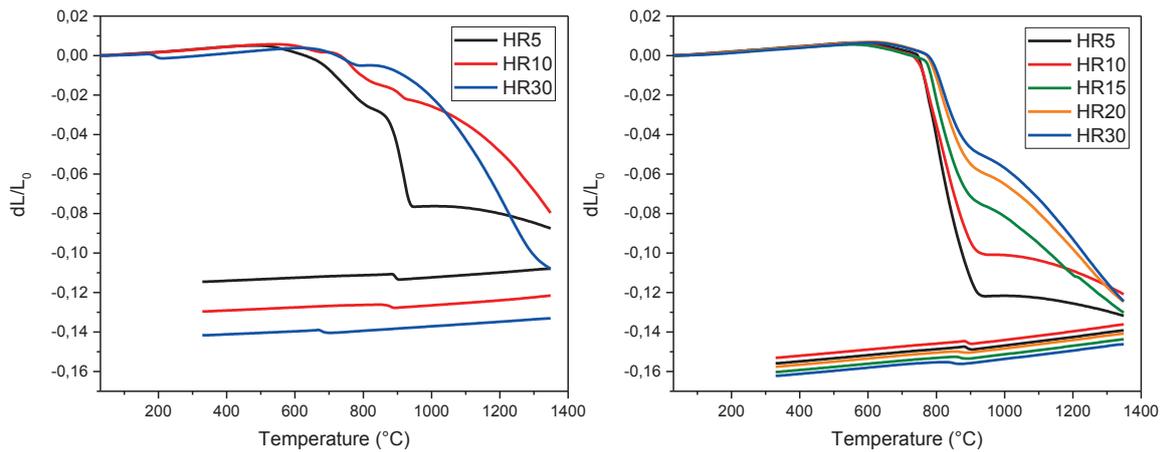

Figure 21: Sintering of carbonyl iron powder grades: a) OM, b) CC.

hydrogen-annealed CC grade, the sintering is more predictable without major compositional effects. A clear change in sintering rate was observed at the transformation temperature.

Chapter VI – Conclusions

Sintering of iron and low-alloyed steels is a complicated process. The outcome is influenced by

- The physical and surface chemical properties of the metal powder
- The initial green state, i.e. the powder compact with its localized deformation, porosity etc.
- Delubrication and how organic material is removed from the powder compact prior to sintering
- Sintering parameters in terms of the effects of the temperature profile and sintering atmosphere properties (composition, purity, etc.) on the powder surface chemistry and therefore sintering behaviour of the powder

The aim of this licentiate thesis was to expand upon the knowledge already present in the field of sintering of iron and low-alloyed steels. In particular, the link between the factors above was investigated.

It was shown that a size dependence exists which determines the extent of enrichment of impurity oxygen-sensitive elements at the surface as a function of particle size. This is turn determines the fraction of interparticle contacts that are initially free of oxides that are difficult to reduce. A connection between the surface iron oxide layer measured by XPS and TGA was found, pointing towards an oxide thickness of 5-7 nm which is in line with previously reported values.

Kinetic analysis provided information about some of the fundamental properties of the surface iron oxide layer and how it behaves in a hydrogen atmosphere. This information can be valuable in determining e.g. the onset of sinter neck formation at different temperatures where diffusion across particles is likely to be favoured if the interparticle contact regions are free of oxygen. Furthermore, diffusion of oxygen from within the powder could be identified, along with its phase dependence. This becomes important as it explains how oxygen is transferred to the surface of the particles and influences the oxide transformation mechanisms. For carbonyl iron powder, the kinetic analysis provided information about the important interactions with the atmosphere, such as reduction of surface oxide and removal and nitrogen and carbon, which corresponds to the break-up of the internal structure of the standard grades.

Water-atomized iron powder is heavily deformed during compaction with a large density of low-angle grain boundaries localized to interparticle regions. Protrusions and small sections on metal particles are likely candidates for deformation and will exhibit a larger volume fraction of deformation than the larger particles or particle sections. This deformed interparticle contact region may affect the self-diffusion properties that govern the early stages of sintering, both via dislocation pipe diffusion mechanisms and an altered and refined grain structure. Low temperature sintering studies of water-atomized iron powder showed a markedly increased sintering activity of highly compacted samples, likely a consequence of the flattened interparticle regions. Furthermore, this effect was particularly pronounced in the high-diffusivity ferrite region, again highlighting the phase dependence of diffusion. Sintering at high temperatures indicated that the effect from compaction was largely kept from the ferrite region.

Sintering of carbonyl iron powder showed a large effect of the heating rate which effectively controls the time spent in each phase. Sintering shrinkages were larger with a high heating rate. At the same time, strong interactions with the atmosphere determine how the chemical composition is changed, further influencing the sintering behaviour.

Chapter VII – Future work

Sintering anisotropy is a challenge for keeping tolerances in powder metallurgical steels. The deformation behaviour of the compacts have been identified as one major cause for this. This topic should be studied more extensively to acquire a more in depth knowledge about how and why the material behaves the way it does. Furthermore, a more generally applicable reasoning could be of interest to utilize the knowledge across material barriers. The recrystallization behaviour of deformed powder metallurgical samples could reveal some of the intricacies connected to the initial state of sintering. The extent of pipe diffusion as a result of highly deformed regions in the interparticle contacts could be studied, along with the newly developed grain structure which could facilitate enhanced grain boundary diffusion. The recrystallization effects could possibly be studied with EBSD, DSC, XRD and microhardness. A more in-depth analysis of powder surfaces and how they change with e.g. compaction and various low-temperature sintering programs could also be important.

Acknowledgements

First and foremost I would like to express my gratitude towards my supervisor Professor Lars Nyborg and Professor Eduard Hryha for providing me with support and guidance throughout the work. Their knowledge about powder is likely endless.

Thanks to Yu Cao and Ruslan Shvab for sharing knowledge and introducing me to surface science, and for being part of my research as co-authors.

Thanks to the people at Höganäs, in particular Dr. Dimitris Chasoglou and (previously) Dmitri Riabov and Sigurd Berg, for helping me by providing powder, chemical analyses, pressing, and injection moulding.

A special thanks to Roger Sagdahl, Håkan Millqvist and Dr. Eric Tam for their willingness to help with practical support if, and when, something breaks down.

I would like to thank all colleagues and members of the department for creating a pleasant and encouraging working environment.

I would especially like to express my thanks to all fellow PhD students, past and present, with whomstd'I've shared this journey for the last few years. A special thanks to the people of the powder group, for mostly fruitful discussions about everything related to particles, and especially the problems they impose on our daily lives. I am particularly grateful to Mahesh and Swathi for all our discussions about the purest and most noble form of powder metallurgy.

I would like to thank my friends not at Chalmers, for reminding me of the outside world.

Lastly, to my family, you are forever in my mind.

References

[1]   W. Schatt, K.-P. Wieters, Powder Metallurgy - Processing and Materials, 1997.

[2]   H. Danninger, C. Gierl, Processes in PM steel compacts during the initial stages of sintering, Mater. Chem. Phys. 67 (2001) 49–55. doi:10.1016/S0254-0584(00)00419-3.

[3]   H. Danninger, C. Gierl, S. Kremel, G. Leitner, Y. Yu, Degassing And Deoxidation Processes During Sintering Of Unalloyed And Alloyed Pm Steels, Powder Metall. Prog. 2 (2002) 125–140.

[4]   H. Danninger, C. Gierl, New alloying systems for ferrous powder metallurgy precision parts, Sci. Sinter. 40 (2008) 33–46. doi:10.2298/SOS0801033D.

[5]   D. Chasoglou, E. Hryha, L. Nyborg, Effect of sintering atmosphere on the transformation of surface oxides during the sintering of chromium alloyed steel, 9 (2009) 141–155.

[6]   E. Hryha, C. Gierl, L. Nyborg, H. Danninger, E. Dudrova, Surface composition of the steel powders pre-alloyed with manganese, Appl. Surf. Sci. 256 (2010) 3946–3961. doi:10.1016/j.apsusc.2010.01.055.

[7]   C. Schade, Surface Modifications of PM Stainless Steels for Enhanced Corrosion Resistance, Powder Metall. 38 (1995) 120–130.

[8]   R.M. German, Sintering Theory and Practice, John Wiley & Sons, New York, 1996.

[9]   L. Parilak, E. Dudrova, R. Bidulsky, M. Kabatova, Quantification of Metal Powder Compressibility in Uniaxial Compaction, Euro PM2004. 1 (2004) 593–598.

[10]   L. Parilak, E. Dudrova, R. Bidulsky, M. Kabatova, Derivation, testing and application of a practical compaction equation for cold die-compacted metal powders, Powder Technol. 322 (2017) 447–460. doi:10.1016/j.powtec.2017.09.027.

[11]   A. Molinari, C. Menapace, E. Torresani, I. Cristofolini, M. Larsson, Working hypothesis for origin of anisotropic sintering shrinkage caused by prior uniaxial cold compaction, Powder Metall. 0 (2012) 1–8. doi:10.1179/1743290112Y.0000000043.

[12]   E. Torresani, Mechanism of anisotropic shrinkage during sintering of metallic powders, (2016).

[13]   A. Zavaliangos, J.M. Missiaen, D. Bouvard, Anisotropy in shrinkage during sintering, Sci. Sinter. 38 (2006) 13–25. doi:10.2298/SOS0601013Z.

[14]   R.M. German, A. Bose, Injection Molding of Metals and Ceramics, Metal Powder Industries Federation, 1997.

[15]   S. Karamchedu, E. Hryha, L. Nyborg, Changes in the surface chemistry of chromium-alloyed powder metallurgical steel during delubrication and their impact on sintering, J. Mater. Process. Technol. 223 (2015) 171–185. doi:10.1016/j.jmatprotec.2015.03.054.

[16]   E. Hryha, E. Dudrova, L. Nyborg, On-line control of processing atmospheres for proper sintering of oxidation-sensitive PM steels, J. Mater. Process. Technol. 212 (2012) 977–987. doi:10.1016/j.jmatprotec.2011.12.008.

[17]   R.M. German, Chapter Two - History of Sintering, Sinter. from Empir. Obs. to Sci. Princ. (2014) 13–40. doi:http://dx.doi.org/10.1016/B978-0-12-401682-8.00002-1.

[18]   A.R. Poster, H.H. Hausnert, Alpha and Gamma Phase Sintering of Carbonyl and Other Iron Powders, (2000) 26–44.

[19]   R.M. German, Chapter One - Introduction, Sinter. from Empir. Obs. to Sci. Princ. (2014) 1–12. doi:10.1016/B978-0-12-401682-8.00001-X.

[20]   H. Danninger, C. Gierl-mayer, Advanced powder metallurgy steel alloys, 2013. doi:10.1016/0026-0657(92)91807-V.

[21]   C. Gierl-Mayer, R. de Oro Calderon, H. Danninger, The Role of Oxygen Transfer in Sintering of Low Alloy Steel Powder Compacts: A Review of the "Internal Getter" Effect, Jom. 68 (2016). doi:10.1007/s11837-016-1819-z.

[22]   E. Hryha, H. Borgström, K. Sterky, L. Nyborg, Influence of the steel powder type and processing parameters on the debinding of PM compacts with gelatin binder, J. Therm. Anal. Calorim. 118 (2014) 695–704. doi:10.1007/s10973-014-3839-7.

[23]   D. Chasoglou, E. Hryha, M. Norell, L. Nyborg, Characterization of surface oxides on water-atomized steel powder by XPS/AES depth profiling and nano-scale lateral surface analysis, Appl. Surf. Sci. 268 (2013) 496–506. doi:10.1016/j.apsusc.2012.12.155.

[24]   D. Chasoglou, E. Hryha, L. Nyborg, Effect of process parameters on surface oxides on chromium-alloyed steel powder during sintering, Mater. Chem. Phys. 138 (2013) 405–415. doi:10.1016/j.matchemphys.2012.11.074.

[25]   T. Yamashita, P. Hayes, Analysis of XPS spectra of Fe2+ and Fe3+ ions in oxide materials, Appl. Surf. Sci. 254 (2008) 2441–2449. doi:10.1016/j.apsusc.2007.09.063.

[26]   BASF, No Title, (2018). https://www.dispersions-pigments.basf.com/portal/basf/em/dt.jsp?setCursor=1_827912 (accessed March 14, 2018).

[27]   B.Y. Tay, L. Liu, N.H. Loh, S.B. Tor, Y. Murakoshi, R. Maeda, Surface roughness of microstructured component fabricated by ??MIM, Mater. Sci. Eng. A. 396 (2005) 311–319. doi:10.1016/j.msea.2005.01.033.

[28]   J.L. Johnson, D.F. Heaney, N.S. Myers, Metal injection molding (MIM) of heavy alloys, refractory metals, and hardmetals, in: Handb. Met. Inject. Molding, 2012: pp. 526–567. doi:10.1533/9780857096234.4.526.

[29]   P. Kofstad, High Temperature Corrosion, 1 edition, Elsevier Applied Science, 1988.

[30]   E. Hryha, L. Nyborg, Thermogravimetry study of the effectiveness of different reducing agents during sintering of Cr-prealloyed PM steels, J. Therm. Anal. Calorim. 118 (2014) 825–834. doi:10.1007/s10973-014-3915-z.

[31]   C. Gierl-Mayer, H. Danninger, Dilatometry Coupled with Mass Spectrometry as Instrument for Process Control in Sintering of Powder Metallurgy Steels, Mater. Sci. Forum. 835 (2016) 106–115. doi:10.4028/www.scientific.net/MSF.835.106.

[32]   R. de Oro Calderon, C. Gierl-Mayer, H. Danninger, Application of thermal analysis techniques to study the oxidation/reduction phenomena during sintering of steels containing oxygen-sensitive alloying elements, J. Therm. Anal. Calorim. (2016). doi:10.1007/s10973-016-5508-5.

[33]   H.E. Kissinger, Reaction Kinetics in Differential Thermal Analysis, Anal. Chem. 29 (1957) 1702–1706. doi:10.1021/ac60131a045.

[34]   H.E. Kissinger, Variation of peak temperature with heating rate in differential thermal analysis, J. Res. Natl. Bur. Stand. (1934). 57 (1956) 217. doi:10.6028/jres.057.026.

[35]   W.K. Jozwiak, E. Kaczmarek, T.P. Maniecki, W. Ignaczak, W. Maniukiewicz, Reduction behavior

of iron oxides in hydrogen and carbon monoxide atmospheres, Appl. Catal. A Gen. 326 (2007) 17–27. doi:10.1016/j.apcata.2007.03.021.

[36] D. Jelić, J. Penavin-Škundrić, D. Majstorović, S. Mentus, The thermogravimetric study of silver(I) oxide reduction by hydrogen, Thermochim. Acta. 526 (2011) 252–256. doi:10.1016/j.tca.2011.10.001.

[37] M. Belgacem, B. Thierry, G. Jean-Claude, Investigations on thermal debinding process for fine 316L stainless steel feedstocks and identification of kinetic parameters from coupling experiments and finite element simulations, Powder Technol. 235 (2013) 192–202. doi:10.1016/j.powtec.2012.10.006.

[38] M.V.C. Sastri, R.P. Viswanath, B. Viswanathan, Studies on the reduction of iron oxide with hydrogen, Int. J. Hydrogen Energy. 7 (1982) 951–955. doi:10.1016/0360-3199(82)90163-X.

[39] D.A. Porter, K.E. Easterling, M.Y. Sherif, Phase Transformations in Metals and Alloys, Third edit, Taylor & Francis Group, 2009.

[40] F.S. Buffington, K. Hirano, M. Cohen, Self diffusion in iron, Acta Metall. 9 (1961) 434–439. doi:10.1016/0001-6160(61)90137-7.

[41] Y. Iijima, Diffusion in high-purity iron: Influence of magnetic transformation on diffusion, J. Phase Equilibria Diffus. 26 (2005) 466–471. doi:10.1361/154770305X66547.

[42] A. Inoue, H. Nitta, Y. Iijima, Grain boundary self-diffusion in high purity iron, Acta Mater. 55 (2007) 5910–5916. doi:10.1016/j.actamat.2007.06.041.

[43] A. Molinari, E. Bisoffi, C. Menapace, J. Torralba, Shrinkage kinetics during early stage sintering of cold isostatically compacted iron powder, Powder Metall. 57 (2014) 61–69. doi:10.1179/1743290113Y.0000000068.

[44] T. Schubert, T. Pieczonka, S. Baunack, B. Kieback, The Influence of the Atmosphere and Impurities on the Sintering Behaviour of Aluminium, EuroPM. (2005) 3–8.

[45] Y. Shima, Y. Ishikawa, H. Nitta, Y. Yamazaki, K. Mimura, M. Isshiki, Y. Iijima, Self-Diffusion along Dislocations in Ultra High Purity Iron, Mater. Trans. 43 (2002) 173–177. doi:10.2320/matertrans.43.173.

[46] H. Föll, Diffusion in iron, (n.d.). https://www.tf.uni-kiel.de/matwis/amat/iss/kap_5/illustr/s5_2_3d.html (accessed May 2, 2018).

[47] H.F. Fischmeister, R. Zahn, The Mechanism of Sintering of a-Iron, (1966) 12–25.

[48] H.H. Hausner, Modern Developments in Powder Metallurgy, 1966. doi:10.1007/978-1-4684-7882-2.

[49] H.F. Fischmeister, Densification and Grain Growth in the Later Stages of Sintering of Alpha-Iron, (1968) 262–283.

[50] R.M. German, Chapter Four - Measurement Tools and Experimental Observations, 2014. doi:http://dx.doi.org/10.1016/B978-0-12-401682-8.00004-5.

[51] A. Molinari, E. Torresani, C. Menapace, M. Larsson, The Anisotropy of Dimensional Change on Sintering of Iron, J. Am. Ceram. Soc. 98 (2015) 3431–3437. doi:10.1111/jace.13852.

[52] M. Pilla, A. Molinari, Effect of process parameters on the dimensional and geometrical precision of PM steel parts PhD student :, (2013).

[53]   A. Molinari, E. Bisoffi, C. Menapace, J.M. Torralba, Shrinkage kinetics during the early stage of sintering: The time depending effective diffusion coefficient, Int. Powder Metall. Congr. Exhib. Euro PM 2013. (2013). http://www.scopus.com/inward/record.url?eid=2-s2.0-84924940557&partnerID=tZOtx3y1.

[54]   P.G. Shewmon, Transformation in Metals, McGraw-Hill Book Company, 1969.

[55]   L.N. Brewer, M. a Othon, L.M. Young, T.M. Angeliu, Misorientation mapping for visualization of plastic deformation via electron back-scattered diffraction., Microsc. Microanal. 12 (2006) 85–91. doi:10.1017/S1431927606060120.

[56]   K.S. Hwang, Y.C. Lu, G.J. Shu, B.Y. Chen, Enhanced densification of carbonyl iron powder compacts by the retardation of exaggerated grain growth through the use of high heating rates, Metall. Mater. Trans. A Phys. Metall. Mater. Sci. 40 (2009) 3217–3225. doi:10.1007/s11661-009-9995-x.

[57]   R.M. German, Chapter Nine - Sintering With a Liquid Phase, 2014. doi:10.1016/B978-0-12-401682-8.00009-4.

[58]   A.R. Annamalai, F. Nekatibeb, A. Upadhyaya, D.K. Agrawal, Effect of heating mode on sinterability of carbonyl iron compacts, Mater. Res. Innov. 17 (2013) 10–16. doi:10.1179/1433075X12Y.0000000011.

[59]   J.L. Meijering, On the diffusion of oxygen through solid iron, Acta Metall. 3 (1955) 157–162. doi:10.1016/0001-6160(55)90085-7.

[60]   R. König, S. Müller, R.E. Dinnebier, B. Hinrichsen, P. Müller, A. Ribbens, J. Hwang, R. Liebscher, M. Etter, C. Pistidda, The crystal structures of carbonyl iron powder – revised using in situ synchrotron XRPD, Zeitschrift Für Krist. - Cryst. Mater. 232 (2017) 835–842. doi:10.1515/zkri-2017-2067.

[61]   M. Norell, L. Nyborg, T. Tunberg, I. Olefjord, Thickness determination of surface oxides on metal powder by AES depth profiling, Surf. Interface Anal. 19 (1992) 71–76.

[62]   H. Karlsson, L. Nyborg, S. Berg, Surface chemical analysis of prealloyed water atomised steel powder, Powder Metall. 48 (2005) 51–58. doi:10.1179/0032589005X37675.

[63]   H. Danninger, C. Gierl-mayer, S. Strobl, Evolution of microstructure in ferrous and non-ferrous materials, 2013. doi:10.1533/9780857098900.2.308.

[64]   H.-Y. Lin, Y.-W. Chen, C. Li, The mechanism of reduction of iron oxide by hydrogen, Thermochim. Acta. 400 (2003) 61–67. doi:10.1016/S0040-6031(02)00478-1.

[65]   F. Scholz, J.. Driver, E. Woldt, The stored energy of cold rolled ultra high purity iron, Scr. Mater. 40 (1999) 949–954. doi:10.1016/S1359-6462(99)00047-0.

[66]   F. Scholz, E. Woldt, The release of stored energy during recovery and recrystallization of cold rolled ultra high purity iron, J. Therm. Anal. Calorim. 64 (2001) 895–903. doi:10.1023/A:1011558511053.